Gondwana Research 27 (2015) 575–593

Contents lists available at ScienceDirect

Gondwana Research

journal homepage: www.elsevier.com/locate/gr

Arc-related harzburgite–dunite–chromitite complexes in the mantle section of the Sabzevar ophiolite, Iran: A model for formation of podiform chromitites

Hadi Shafaii Moghadam [a,1], Mohamed Zaki Khedr [b,c], Shoji Arai [b], Robert J. Stern [d], Ghasem Ghorbani [a], Akihiro Tamura [b], Chris J. Ottley [e]

[a] School of Earth Sciences, Damghan University, Damghan, Iran
[b] Department of Earth Sciences, Kanazawa University, Kanazawa 920-1192, Japan
[c] Department of Geology, Faculty of Science, Kafrelsheikh University, Egypt
[d] Geosciences Dept., University of Texas at Dallas, Richardson, TX 75083-0688, USA
[e] Northern Center for Isotopic and Elemental Tracing, Department of Earth Sciences, University of Durham, Durham DH1 3LE, UK

ARTICLE INFO

Article history:
Received 18 February 2013
Received in revised form 6 September 2013
Accepted 8 September 2013
Available online 1 October 2013

Keywords:
Podiform chromitite
Geochemistry
Melt–mantle interaction
Sabzevar ophiolite

ABSTRACT

Podiform chromitites are common within the mantle section of the Late Cretaceous Sabzevar ophiolite in NE Iran. We studied chromitite pods and related ultramafic rocks from three Sabzevar massifs: Baghjar-Kuh Siah, Gaft Chromitite Mine and Forumad peridotite–chromitite. These represent an upper mantle sequence just below the Sabzevar Moho. The Baghjar-Kuh Siah mantle sequence contains plagioclase lherzolites, enriched in bulk REEs, with low Cr# spinels and MORB-like clinopyroxenes. These lherzolites formed due to the impregnation of MORB-like melts. The Gaft and Forumad harzburgites are depleted in trace and rare earth elements and thus are residues after high degree of partial melting (more than exhaustion of Cpx). The Gaft Chromitite Mine includes two types of podiform chromitites, high Cr# and low Cr#. The melt precipitating high Cr# spinel was boninitic whereas the melt forming the low Cr# chromitites was tholeiitic. Most Forumad massif chromitites have high Cr# spinels, although those rich in silicate inclusions are aluminous. Trace and REE element patterns of Forumad harzburgite clinopyroxene are similar to those in supra-subduction zone (SSZ) peridotites while those of Baghjar-Kuh Siah lherzolites are similar to MOR peridotite clinopyroxenes. These mineral data are also consistent with bulk rock trace and rare earth elements composition of their host peridotites. Field observations indicate that early tholeiitic magmas were followed by late boninites, as revealed in chromitite compositions as well as mantle rocks and dikes. We suggest a time-integrated model for the evolution of the Sabzevar mantle sequence during an early stage of subduction initiation associated with formation of an incipient arc. In this scenario, MORB-like melts (forearc basalts) formed first, causing low Cr# chromitites and plagioclase–clinopyroxene impregnations. Subsequent arc-like or boninitic melts with increasing contribution of slab-derived fluids were responsible for the formation of replacive dunites and high Cr# chromitites.

1. Introduction

Geochemical data from ophiolitic as well as abyssal peridotites and their constituent minerals give new insights into our understanding of melt extraction, melt–mantle interaction, mantle depletion and heterogeneity in the upper mantle (e.g., Niu et al., 1997; Uysal et al., 2012; Zaki Khedr et al., 2013). This data also can provide information about the original tectonic setting where the ophiolite formed (e.g., Bizimis et al., 2000; Pearce et al., 2000; Aldanmaz et al., 2009). Mantle peridotites may originate in a variety of tectonic environments such as mid-ocean ridge (MOR) and supra-subduction zone (SSZ) settings. Mantle residues from these tectonic settings can often be distinguished by the record of the melting regime they experienced as reflected in their bulk and mineral compositions including the presence or absence of chromitite deposits. Although partial melting is the main factor in the mantle heterogeneity, other factors such as melt–mantle interaction can also produce significant geochemical heterogeneity (e.g., Kelemen et al., 1992; Aldanmaz et al., 2009; Uysal et al., 2012).

The presence or absence of podiform chromitite bodies is an important petrotectonic indicator (Rollinson and Adetunji, 2013a,b). Fertile mantle usually lacks podiform chromitites whereas depleted mantle often hosts such bodies. Ophiolitic podiform chromitites are common within harzburgite–dunite dominated mantle sections and mantle–crust transition zones (Moho Transition Zone, MTZ) (Arai, 1997a, 1997b), especially in supra-subduction zone ophiolites. They are rarely found in the crustal section of ophiolites, where they are associated

E-mail address: hadishafaii@du.ac.ir (H. Shafaii Moghadam).
[1] Tel.: +98 9132762361.

1342-937X/$ – see front matter
http://dx.doi.org/10.1016/j.gr.2013.09.007

with late dunitic intrusions (Arai et al., 2004). Podiform chromitites are typically accompanied by abundant dunitic pods and mafic dikes and their origin is thought to be related to extensive melt/rock (peridotite) interaction and subsequent melt–mantle mixing (e.g., Zhou et al., 1996; Arai et al., 1997; Zhou et al., 1998, 2005). These types of chromitites are compositionally either low Cr# (Al_2O_3 > 25 wt.%) or high Cr# (Cr_2O_3 = 45–60 wt.%) varieties (e.g., Leblanc and Violette, 1983; Hock et al., 1986; Zhou and Robinson, 1994). Low Cr# chromitites are commonly associated with troctolitic dikes and may have crystallized from MORB-like tholeiitic melts (Zhou and Robinson, 1994, 1997; Zhou et al., 1998, 2001), while high Cr# chromitites are reported from arc-related setting and are thought to form from boninitic magmas (Arai and Abe, 1994; Arai, 1997a, 1997b). Based on the occurrence of high pressure minerals such as diamond and coesite, podiform chromitites were recently subdivided into ultra-high pressure (UHP) chromitites (e.g., Robinson et al., 2004; Yang et al., 2007; Yamamoto et al., 2009; Miura et al., 2012) and low pressure chromitites. Arai et al. (2010) interpreted UHP chromitites as deep recycling materials, i.e., low pressure chromitites subducted deep into the mantle which then reappeared beneath a spreading center. Podiform chromitites can be classified in the field into two types; concordant and discordant, based on the structural relationship with host mantle peridotite foliation (Cassard et al., 1981). Ahmed and Arai (2002) and Miura et al. (2012) recognized that two different magmas produced discordant and concordant podiform chromitites from Wadi Hilti, northern Oman ophiolite; MORB-type magma for the concordant chromitites and hydrous, boninite-type magma for the discordant chromitites.

In this paper, we report results of the first study of mantle peridotites and podiform chromitites in the mantle section of the Late Cretaceous Sabzevar ophiolite in NE Iran (Fig. 1). We show that i) there is mantle heterogeneity in this region, with variably depleted residues after partial melting and impregnated peridotites due to the melt–rock interaction and ii) there are two distinct chromitite varieties, characterized by different modes of occurrence and Cr–Al content. We discuss results from three regions, separated by several tens of kilometers (Fig. 2): a) Baghjar-Kuh Siah, the easternmost; b) Gaft Chromitite Mine and c) Forumad region, the westernmost. Field observation, petrography, and major-trace elements data for bulk peridotites as well as chromitites and related silicate minerals are presented and discussed. We use these data to model the origin of the two chromitites based on inferred types of parental melts and melt–peridotite reactions.

2. Geological background

Two major belts of ophiolites decorate suture zones in the Iranian plateau: a) the Paleozoic ophiolite belt (Paleotethys remnants) and

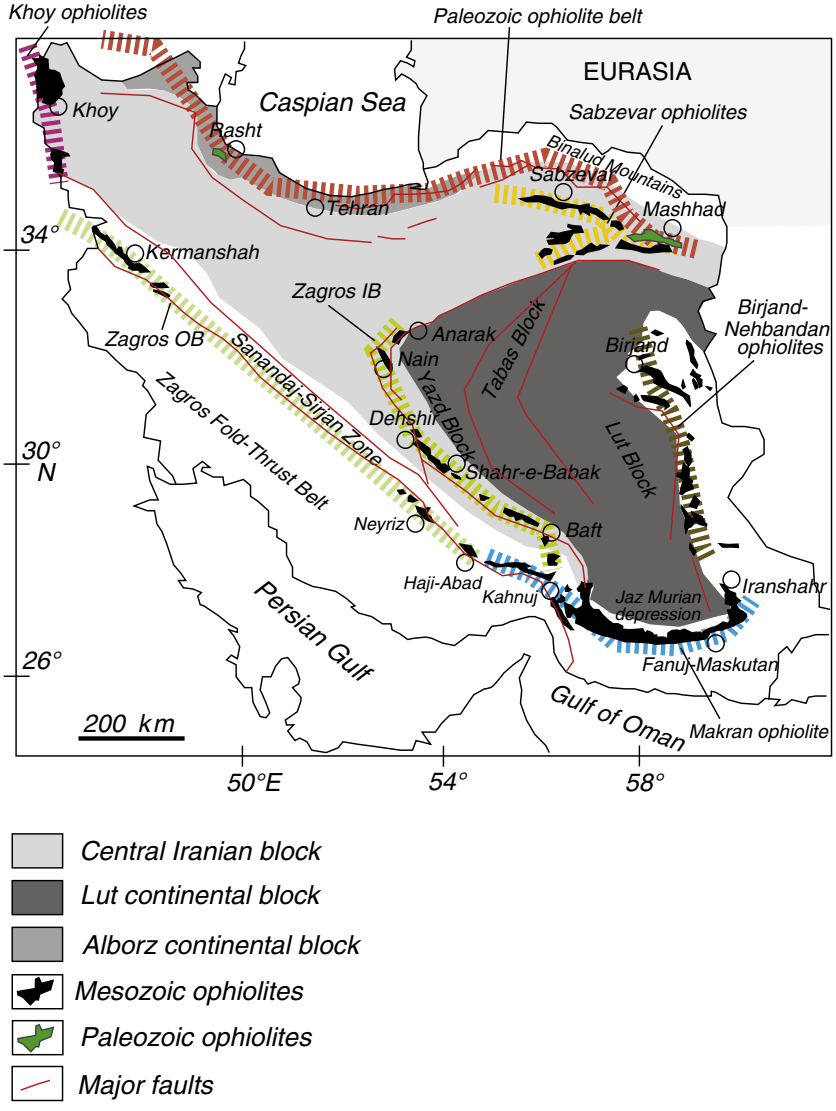

Fig. 1. Simplified geological map of Iran emphasizing two main ophiolitic belts (thick dashed lines); 1) Paleozoic ophiolites and 2) Mesozoic ophiolites including Khoy ophiolites, outer and inner Zagros ophiolite belts, Makran ophiolites, Birjand-Nehbandan ophiolites and Sabzevar ophiolite.

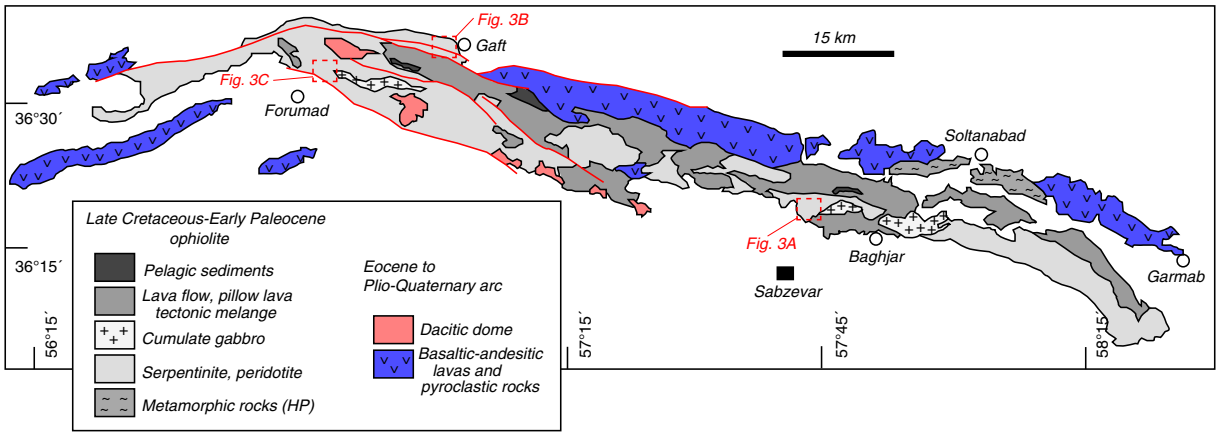

Fig. 2. Simplified geological map of the Sabzevar–Forumad ophiolites, N–NW of Sabzevar town. Note locations of 3 regions studied here. Modified after Sabzevar and Forumad 1/100000 geological maps.

b) the Mesozoic ophiolite belt (Neotethys remnants) (Fig. 1). Paleozoic ophiolites are mainly distributed in northern Iran, defining the suture between the Turan (Eurasia) and the Iranian Cimmerian blocks (Central Iranian and Alborz blocks) where Paleotethys was consumed by subduction beneath southern Eurasia (Alavi, 1991). The Sabzevar ophiolite is part of the Mesozoic ophiolite belt and is situated in NE Iran (Fig. 1) between the Lut Block to the south and the Binalud mountains to the north. The exposed ophiolite is about 150 km long and 10–30 km wide. The Sabzevar ophiolite is considered to represent the northern branch of the Neotethys Ocean (the Sabzevar Ocean) that opened and closed during the Late Cretaceous and may be related to the ophiolites of the Lesser Caucasus (Lensch, 1980; Sengor, 1990). Berberian and King (1981) considered that the Sabzevar ophiolite, like the Nain-Baft ophiolites of Zagros, is related to a seaway surrounding the Lut Block. Noghreyan (1982) suggested that the Sabzevar ophiolitic rocks formed in a back-arc basin, based on the geochemistry of lavas and gabbros (Baghjar region, Fig. 2). Recent U–Pb zircon dating (Shafaii Moghadam et al., unpublished data) yielded ages of ca. 100–78 Ma for Sabzevar plagiogranites. Zircon and titanite U–Pb geochronology on felsic segregations in ophiolite-related blueschists and retrogressed mafic granulites yielded ages of 107.4 ± 2.4 and 105.9 ± 2.3 Ma (Albian) respectively (Rossetti et al., 2010).

This ophiolite is overlain by Upper Cretaceous to Paleocene extrusive rocks, associated with volcaniclastic sediments, pelagic limestone and radiolarian chert. Shojaat et al. (2003) recognized three chemical varieties of extrusive rocks: 1) N-MORB type basalts and gabbros; 2) E-MORB type basalts and 3) basalts with arc signature. Maleki (2013) subdivided the crustal sequence differently, with calc-alkaline, IAT and OIB-type pillowed and massive basalts.

Baroz and Macaudiere (1984) distinguished four lithostratigraphic units in the ophiolite, from Campanian at the base to Paleocene in the upper parts, with alkaline to calc-alkaline pillow lavas, litharenites, breccias and agglomerates with pelagic sediments. Harzburgite, lherzolite, dunite and chromitite are the major components of the Sabzevar mantle sequence. Mantle peridotites are crosscut by abundant diabasic and gabbroic dikes. Sabzevar gabbroic rocks are divided into both

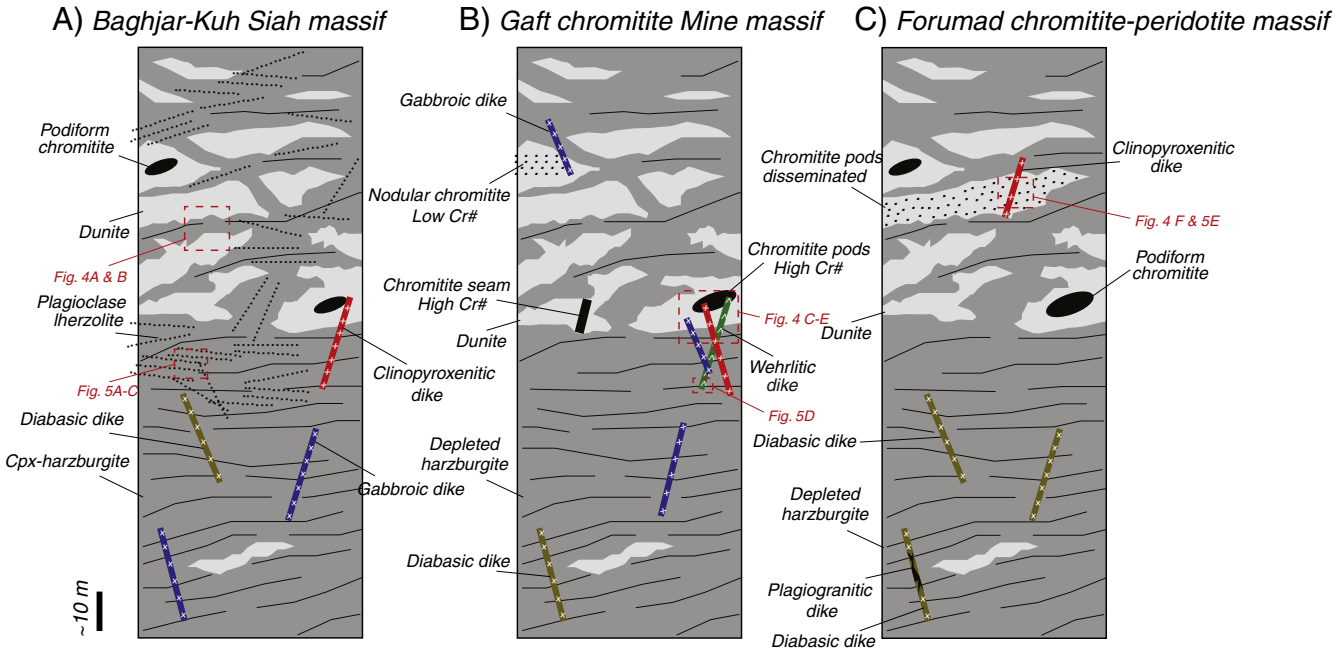

Fig. 3. Schematic cross sections (based on the field work) of the Baghjar-Kuh Siah, Gaft Chromitite Mine and Forumad mantle columns showing the relationships between rock units in the mantle transition zones studied here.

isotropic gabbroic lenses within mantle harzburgites and cumulate layered gabbro–gabbronorite as part of the crustal section. A fragmented and sheared sheeted dike complex, with early basaltic to andesitic basaltic dikes and late dacitic dikes, is exposed near Baghjar village (Fig. 2).

Large masses of peridotite with podiform chromitite are distributed in the central and western parts of the Sabzevar ophiolite and are especially well-developed in three regions; the Baghjar-Kuh Siah region (Appendix 1), the Gaft Chromitite Mine, and the Forumad massif (Appendix 2 and Fig. 3). There are a lot of ancient and recent chromite mines in the region, but most are inactive due to the small deposit size; for example, the deserted Baghjar, Ayvaz, Tutsang, Sang-Sefid mines each contain <300 tons of ore. The only active mines are located NW of Sabzevar town, in the Forumad and Gaft regions. Important active mines in this region are Sarvar mines (including Nosrati, Arian), Char Tayeb, and Masih-Abad deposits, the larger ones containing about 5000 tons of ore materials. There are also several very small mines, with 3–4 tons of ore.

3. Geology and petrography of chromitites and host peridotites

3.1. Baghjar-Kuh Siah peridotite massif (central part of the ophiolite)

This massif consists chiefly of harzburgite and lherzolite with variably sized (20–30 cm but mostly >1 m wide) lenses and dikes of dunite, discordant–subconcordant to the tectonic fabric of host peridotites including high temperature foliation, represented by alignment of stretched orthopyroxene, but rarely spinel grains (Figs. 3 and 4A, B). The relationship between harzburgite and dunite, including preservation of pyroxene-rich domains within dunites, is similar to that seen in the Oman ophiolite, which has been interpreted as forming by in-situ replacement due to the melt/rock interaction and subsequent

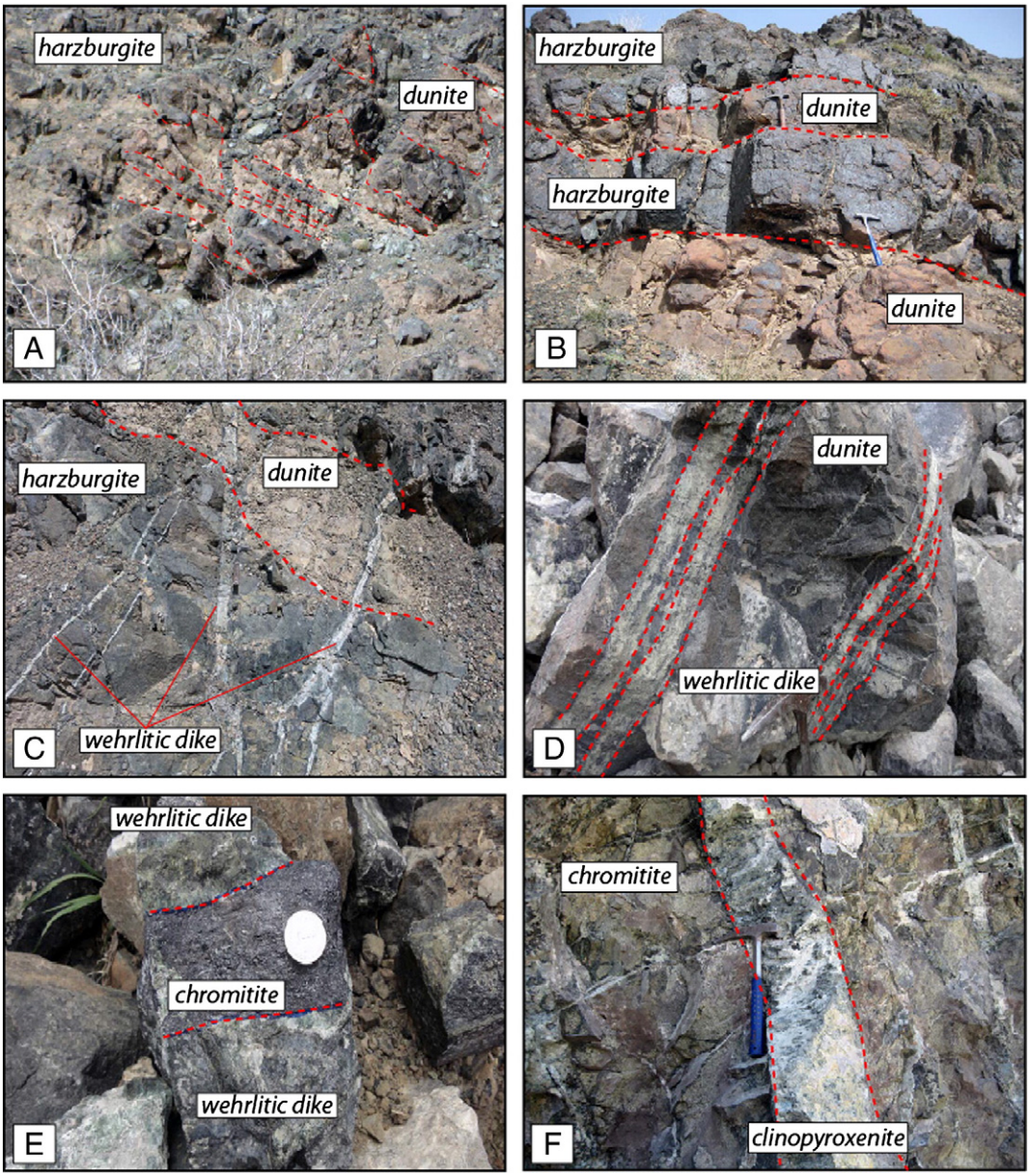

Fig. 4. Field photographs of the Baghjar-Kuh Siah; Gaft Chromitite Mine and Forumad ophiolites. A and B — Lenses and layers (dikes) of dunite, discordant-subconcordant to the tectonic fabric of host peridotites, in the mantle section of the Baghjar-Kuh Siah peridotite massif. C, D and E — The occurrence of dunitic lenses within mantle harzburgites of the Gaft Chromitite Mine peridotite massif associated with injection of early wehrlitic dikes that crosscut all units including mantle depleted harzburgites, dunites (C, D) and chromitites (E). F — Pegmatite clinopyroxenitic dike crosscutting podiform chromitites and dunites in the Forumad peridotite–chromitite massif.

incongruent orthopyroxene melting (Kelemen et al., 1992). Podiform chromitites are found within depleted harzburgites, typically enveloped by dunite. Small (4–5 mm, rarely 2–3 cm) wehrlitic veins are common within the Kuh Siah mantle sequence. Lherzolites, harzburgites and dunites are serpentinized with the degree of serpentinization ranging from ~10% (in plagioclase lherzolites) to >80% (dunites). Harzburgites consist of olivine, large orthopyroxene porphyroclasts and spinel with rare clinopyroxene. Olivine is anhedral and occasionally shows typical kink-band deformation. Orthopyroxene occurs as subhedral to generally tabular grains. Dunites are strongly serpentinized and only a few relicts of olivine and spinel survive. Lherzolites are most common in the Kuh Siah massif and have gradational contacts with harzburgites. Most lherzolites show melt-pocket shaped domains (Fig. 5A), consisting chiefly of large clinopyroxene, olivine and vermicular, light brown (Al-rich) spinels. These pockets are generally characterized by coarse-grained crystals forming equigranular texture (Fig. 5A). These pockets resemble older mantle wehrlitic intrusions/melt impregnations that now are subconcordant to host peridotite foliation. These structures are not observed in dunitic lenses within lherzolites in the Baghjar-Kuh Siah region, so these dunites must have formed later, after melt percolation. Lherzolites have anhedral olivines, large orthopyroxene porphyroclasts (~5–6 mm, up to 10 mm), and smaller clinopyroxene grains (Fig. 5B). Vermicular light brown spinels are common. Lherzolites also contain small, anhedral blebs of plagioclase (usually highly saussuritized), interstitial between olivine and orthopyroxene, surrounding the large spinel grains and/or crosscutting clinopyroxene or spinel grains (Figs. 5C, 6A–B).

Chromitites are mainly tabular or lensoid and are discordant to the mantle fabric. Chromitites show massive (>70 vol.% chromite) or disseminated textures. Fine-grained disseminated chromitites are

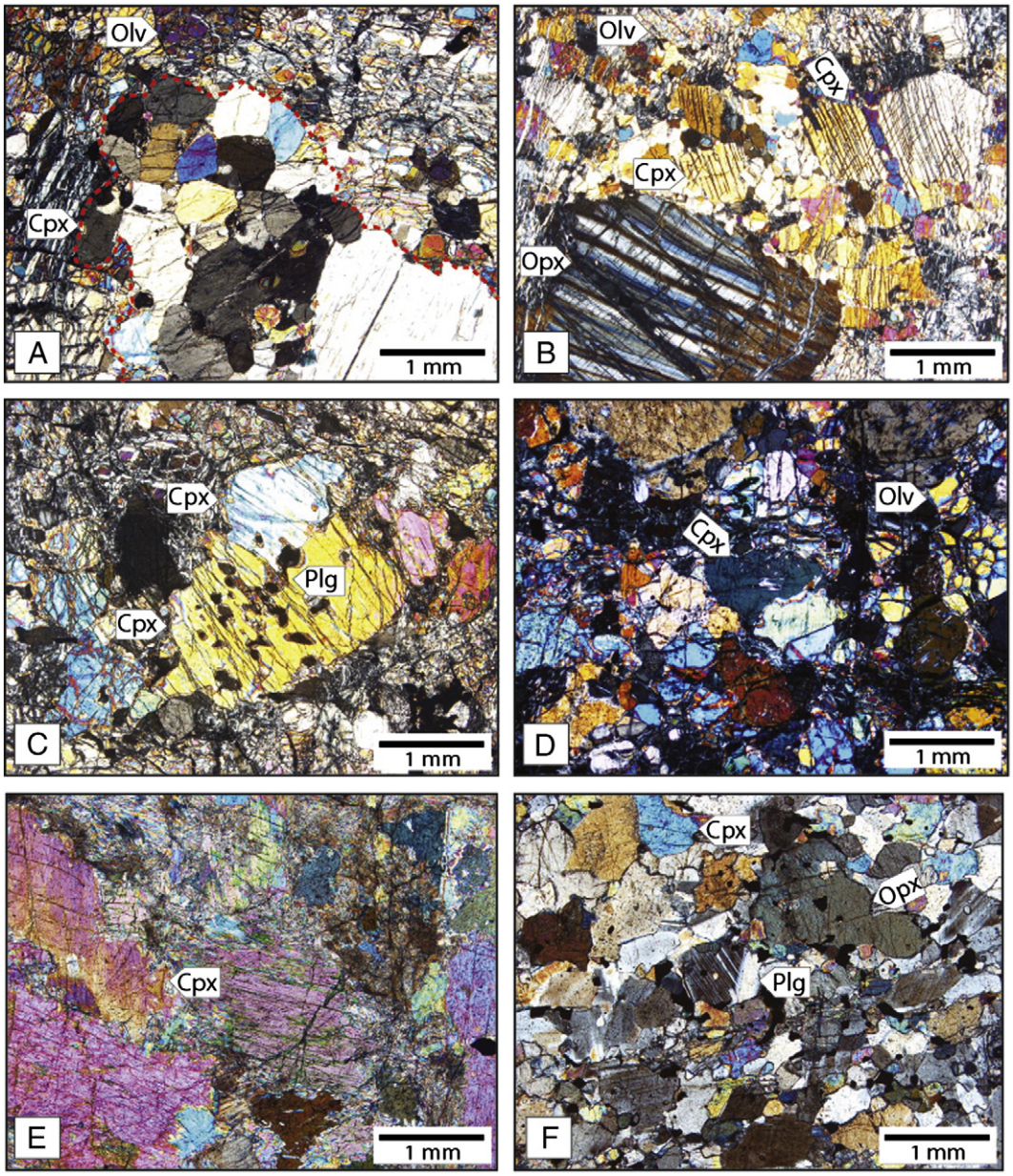

Fig. 5. Microphotographs of the Baghjar-Kuh Siah, Gaft Chromitite Mine and Forumad mantle rocks. A — Large clinopyroxene and olivine (associated with vermicular spinels) as melt-pocket shaped domains (outlined by red dashed line) in the Baghjar-Kuh Siah lherzolite. B — Small clinopyroxene and olivine grains around large orthopyroxene porphyroclast in the Baghjar-Kuh Siah lherzolite. C — Anhedral blebs of plagioclase (usually highly saussuritized) in clinopyroxene grains of the Baghjar-Kuh Siah lherzolite. D — Association of clinopyroxene, olivine and rare orthopyroxene in early wehrlitic dikes of the Gaft Chromitite Mine peridotite massif. E — Large clinopyroxene grains in clinopyroxenitic dikes, crosscutting Forumad podiform chromitites. F — Small clinopyroxene and orthopyroxene associated with plagioclase laths in late gabbroic dikes of the Gaft mine peridotite massif.

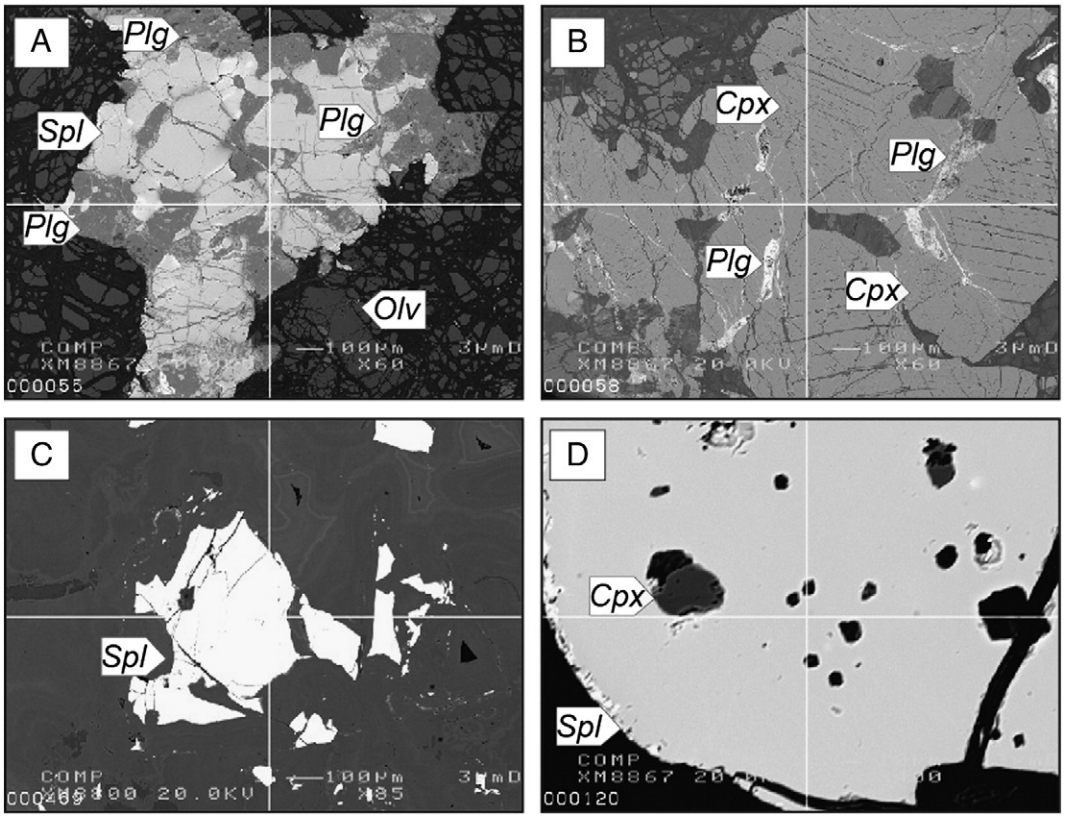

Fig. 6. Back-scattered electron images of the Baghjar-Kuh Siah plagioclase-bearing lherzolites (A and B), Forumad dunites and chromitites (C and D). Small, anhedral blebs of plagioclase surrounding large spinels (A) and/or crosscutting clinopyroxene grains (B). C — Anhedral, large accessory chromite grain in the Forumad dunites. D — Inclusions of pyroxene in chromite grains from the Forumad chromitites.

found at the contact of the massive chromitites with host dunite. Serpentinized olivine is the most abundant silicate mineral in the disseminated chromitites and occurs both as a matrix mineral and as inclusions within chromite grains. Clinopyroxenitic dikes (containing large (7–8 mm) clinopyroxenes and rare olivine) crosscut both the chromitites and host peridotites.

3.2. Gaft Chromitite Mine peridotite massif (northwestern part of the ophiolite)

Peridotites at the Gaft Chromitite Mine are mainly harzburgite and dunite (Fig. 3). Serpentinized olivines associated with orthopyroxene porphyroclasts and subhedral spinels are the main harzburgite components. Rare clinopyroxene relics are found in the harzburgites. Dunites occur as discordant lenses within the harzburgites (Fig. 4C) and/or as thick veins (>1 m width) enveloping chromitite pods. These rocks are strongly serpentinized and olivine and spinel are rarely preserved. Rare clinopyroxene impregnations are present in dunitic lenses, mainly at the contact with wehrlitic dikes. Lherzolites are not known from the Gaft Chromitite Mine peridotite massif. Three main chromitite textures are recognized: 1) massive and densely disseminated pods and lenses (2–3 m in size) that are characterized by chromian spinel modal abundance ranging from 50 to 100 vol.%; 2) irregular seams of massive chromitite 20–30 cm thick in depleted harzburgite/dunites; and 3) nodular chromitites characterized by small (1–2 cm) balls of massive chromian spinel in host dunites. Spinels from Gaft mine chromitites are sieved by clinopyroxene inclusions (usually converted into tremolite) or, more commonly, they are inclusion-free.

Dikes are abundant in the Gaft Chromitite Mine mantle section and can be grouped into five types based on composition and relative age: 1) early wehrlitic dikes that crosscut all units including mantle harzburgites, dunites (both layers in harzburgites and envelope around the chromitites) and chromitites (Fig. 4C, D, E). These dikes vary from thin (2–3 mm) to thick varieties (30 cm). They contain clinopyroxene (>70–80 vol.%), serpentinized to fresh olivine, rare orthopyroxene (<2 vol.%) and small (av. 0.2–0.3 mm) euhedral to subhedral spinel grains (Fig. 5D). The dike texture is usually orthocumulate. 2) Gabbroic dikes that mostly crosscut the early wehrlitic dikes and contain clinopyroxene and highly altered plagioclase. 3) Late-stage gabbronoritic dikes that are characterized by small clinopyroxene and orthopyroxene associated with fresh plagioclase laths (Fig. 5F). These clearly crosscut the gabbroic dikes, but we could not see in the field if they crosscut the chromitites. 4) Clinopyroxenitic dikes that crosscut the early wehrlitic dikes, harzburgites and chromitites. We are unsure if they crosscut gabbroic or gabbronoritic dikes. These dikes contain large (4–5 mm) clinopyroxene grains with rare serpentinized olivines (5–6 vol.%). Clinopyroxene is altered to tremolite. And 5) diabasic dikes which only crosscut mantle harzburgites. Diabasic dikes do not intersect other types of dikes so their relative age is not clear.

The occurrence of depleted peridotites, dunitic lenses, podiform chromitites and wehrlitic intrusions as well as gabbroic–pyroxenitic dikes is reminiscent of a MTZ, similar to what has been described in the Oman ophiolite (e.g., Nicolas, 1989; Akizawa et al., 2012). Layered gabbros are missing in the Gaft Chromitite Mine massif.

3.3. Forumad peridotite–chromitite massif (southwest of the Gaft Chromitite Mine)

The Forumad mantle section consists chiefly of harzburgite with small (20–30 cm; max. 1 m) bands and lenses of dunite (Fig. 3). Harzburgites contain partially serpentinized olivines, many of which show typical kink-band textures. Orthopyroxene forms subhedral, tabular grains with clinopyroxene exsolution lamellae. Accessory chromite grains are anhedral to subhedral. Small (1–2 mm) grains of anhedral

clinopyroxene (<2 vol.%) are common in harzburgites. Dunites show strong serpentinization and relict olivines are rare. Coarse (~1 mm) accessory spinel is typically euhedral to anhedral (Fig. 6C). Podiform chromitites are hosted in depleted (orthopyroxene-poor) harzburgites and enveloped by thin (20–30 cm) dunite. Chromitites are mainly lenses (ave. 3–4 m) and are discordant with host peridotites (e.g., in the Forumad mine). Forumad podiform chromitites have massive (>80%) anhedral, coarse chromian spinel grains. At the Char Tayeb Mine, thick (>10 m), subconcordant seams of dunites with podiform chromitites are hosted by depleted harzburgite. Char Tayeb chromitites are mostly disseminated (30–60 vol.% chromite) with coarse chromian spinel grains. Spinels are frequently aligned, forming trains that are a few centimeters thick. Brecciation is common and nodular textures are rare. The most abundant phase in the chromitite matrix is serpentine without definite textures except for minor batiste pseudomorph after orthopyroxene, but relict olivines occasionally are recognized. Inclusions of pyroxene, hydrous minerals (tremolite) and serpentinized olivines are present in the Forumad chromian spinels (Fig. 6D). There are three types of dikes in the Forumad massif; 1) early diabasic dikes, crosscutting the mantle harzburgites, 2) late plagiogranitic dikes injected into diabasic dikes and 3) pegmatite clinopyroxenitic dikes (10–30 cm and rarely ~1 m thick), with large (usually 5–6 mm but even >4–5 cm) clinopyroxene (Fig. 4E) and rare intercumulus olivines (serpentinized) crosscutting the dunites and podiform chromitites (Fig. 4F). Pegmatitic dikes do not intersect the earlier dikes so the relative age of these are unknown.

4. Analytical methods

Samples were collected from the three areas, mostly from the Gaft Chromitite Mine and from 2 to 3 mines in the Baghjar-Kuh Siah and in Forumad regions. Major element analysis of representative Sabzevar peridotites was performed at ALS lab (Canada) using ICP-AES method (Table 1). Concentration of the REE (rare earth elements) and other trace elements in the Sabzevar peridotites were determined by Inductively Coupled Plasma Mass Spectroscopy (ICP-MS) using a Thermo Scientific X-Series 2 at the Department of Earth Sciences at the University of Durham, following a standard nitric and hydrofluoric acid digestion (Ottley et al., 2003) (Table 1). Sample preparation was undertaken in clean air laminar flow hoods. Briefly the procedure is as follows: into a Teflon vial 4 ml HF and 1 ml HNO_3 (SPA, ROMIL Cambridge) are added to 100 mg of powdered sample, and then the vial is sealed and left on a hot plate at 150 °C for 48 h. Then care was taken to convert insoluble fluorides into soluble nitrate species, using the following procedure: acid mixture was evaporated to near dryness, and then 1 ml HNO_3 was added to the moist residue and was evaporated again to near dryness.

Table 1
Representative whole rock composition of Baghjar-Kuh Siah (SZ-), Gaft mine (GA-) and Forumad (FR-) peridotites.

Sample	Fr11-26	Fr12-48	GA12-11	GA12-13	GA12-15	GA12-16	GA12-27	SZ11-125	SZ11-127	SZ11-101	SZ11-182	SZ11-185
SiO_2	34.91	36.01	50.25	35.22	35.73	35.16	33.84	42.00	43.70	42.40	35.60	35.70
Al_2O_3	0.60	0.42	1.56	0.21	0.79	0.29	0.19	0.58	2.19	2.25	0.04	0.02
FeOt	7.04	7.22	4.09	7.55	7.47	8.00	7.47	7.87	8.37	8.23	7.54	7.39
CaO	1.09	0.61	15.95	0.52	0.61	0.71	0.79	0.60	2.33	2.24	0.12	0.10
MgO	43.43	45.11	25.95	43.23	40.83	43.27	42.82	40.30	37.30	36.40	41.30	41.40
Na_2O	0.01	<0.01	0.24	<0.01	<0.01	<0.01	<0.01	0.01	0.05	0.07	0.01	0.01
K_2O	<0.01	<0.02	0.02	<0.01	0.03	<0.01	<0.01	<0.01	<0.01	<0.01	<0.01	<0.01
Cr_2O_3	0.30	0.25	0.48	0.27	0.25	0.30	0.24	0.37	0.37	0.34	0.30	0.32
TiO_2	0.014	0.004	0.113	0.002	0.004	0.007	0.009	0.0091	0.0380	0.0431	0.0012	0.0007
MnO	0.11	0.12	0.10	0.12	0.13	0.12	0.12	0.10	0.11	0.10	0.08	0.08
P_2O_5	<0.01	<0.01	<0.01	<0.01	<0.01	<0.01	<0.01	0.02	<0.01	0.01	<0.01	0.01
LOI	11.93	9.70	1.20	12.28	13.42	11.52	13.94	9.29	6.69	7.19	14.90	15.60
Total	99.41	99.42	99.92	99.38	99.25	99.35	99.40	101.00	101.00	99.30	99.90	100.50
Sc	9.4630	9.1520	53.4400	6.1090	6.7960	7.5070	5.9960	6.9700	10.9700	10.3500	2.5860	2.4960
V	37.5300	26.6700	110.4000	19.8300	21.6700	31.9800	22.5600	26.3600	54.4100	54.7900	9.7200	1.5780
Mn	0.1110	0.1250	0.0970	0.1240	0.1270	0.1350	0.1290	0.1085	0.1101	0.1114	0.0903	0.0911
Co	102.8000	110.9000	34.7900	106.9000	103.0000	108.1000	107.2000	108.50	97.77	99.05	103.00	103.20
Ni	1725.0000	1957.0000	462.7000	1998.0000	1793.0000	2218.0000	2112.0000	2433.00	2035.00	2041.00	2419.00	2319.00
Rb	0.1430	0.1130	0.6770	0.0690	0.2060	0.0910	0.0850	0.0690	0.2373	0.1756	0.0240	0.0230
Sr	5.5470	2.6600	18.4900	6.8510	14.6700	8.1710	11.8100	9.8600	7.5560	0.5156	3.9810	7.7520
Y	0.4080	0.1900	5.7970	0.0420	0.1330	0.1160	0.1700	0.1774	1.5540	1.8540	0.0110	0.0105
Zr	0.3000	0.2740	10.3800	0.0990	0.1680	0.0950	0.1320	0.0737	0.2762	0.2564	0.0395	0.0356
Nb	0.0510	0.0220	0.1130	0.0130	0.0140	0.0070	0.0140	0.0119	0.0276	0.0082	0.0170	0.0054
Cs	0.1650	0.1120	0.0950	0.0120	0.1040	0.0180	0.0200	0.0308	0.0689	0.0476	0.0142	0.0148
Ba	0.5020	2.9630	2.1020	0.6590	1.4330	0.6890	0.9750	0.5322	0.4314	0.0937	0.1111	0.1301
La	0.0200	0.0050	1.5350	0.0420	0.0040	0.0020	0.0150	0.0027	0.0033	0.0037	0.0004	0.0007
Ce	0.0400	0.0130	4.0870	0.0420	0.0180	0.0050	0.0170	0.0014	0.0039	0.0076	0.0042	0.0029
Pr	0.0050	0.0010	0.6580	0.0040	0.0020	0.0010	0.0020	0.0009	0.0034	0.0053	0.0003	0.0003
Nd	0.0210	0.0040	2.7890	0.0100	0.0130	0.0080	0.0120	0.0329	0.0785	0.0737	0.0136	0.0117
Sm	0.0065	0.0010	0.6650	0.0020	0.0055	0.0030	0.0075	0.0039	0.0568	0.0662	0.0002	0.0004
Eu	0.0025	0.0010	0.2335	0.0010	0.0020	0.0020	0.0025	0.0019	0.0269	0.0316	0.0000	0.0000
Gd	0.0150	0.0030	0.7530	0.0020	0.0060	0.0070	0.0100	0.0092	0.1389	0.1591	0.0002	0.0002
Tb	0.0050	0.0030	0.1340	0.0000	0.0050	0.0000	0.0000	0.0024	0.0298	0.0352	0.0000	0.0000
Dy	0.0430	0.0075	0.8705	0.0040	0.0060	0.0135	0.0245	0.0212	0.2303	0.2652	0.0007	0.0007
Ho	0.0140	0.0050	0.1900	0.0000	0.0040	0.0040	0.0050	0.0056	0.0547	0.0633	0.0002	0.0003
Er	0.0435	0.0085	0.5355	0.0050	0.0060	0.0140	0.0180	0.0205	0.1654	0.1902	0.0017	0.0018
Tm	0.0080	0.0040	0.0890	0.0010	0.0020	0.0030	0.0040	0.0054	0.0277	0.0316	0.0009	0.0009
Yb	0.0690	0.0210	0.5745	0.0105	0.0135	0.0205	0.0250	0.0311	0.1891	0.2150	0.0051	0.0041
Lu	0.0130	0.0050	0.0950	0.0030	0.0030	0.0050	0.0040	0.0060	0.0319	0.0359	0.0014	0.0012
Hf	0.0085	0.0045	0.3035	0.0025	0.0025	0.0025	0.0035	0.0034	0.0250	0.0332	0.0012	0.0011
Ta	0.0420	0.0480	0.0280	0.0220	0.0240	0.0190	0.0230	0.0035	0.0018	0.0010	0.0008	0.0008
Pb	0.0797	0.3747	0.3993	12.6500	36.8900	0.1077	0.1627	0.0293	0.0015	0.0149	0.0059	0.0103
Th	0.0050	0.0020	0.0510	0.0020	0.0010	0.0000	0.0010	0.0162	0.0058	0.0142	0.0099	0.0084
U	0.0010	0.0020	0.0130	0.0260	0.0130	0.0000	0.0010	0.0015	0.0004	0.0008	0.0005	0.0004

Table 2
Trace and rare earth element composition of Cpx from Baghjar-Kuh Siah, Gaft Chromitite Mine and Forumad peridotites and clinopyroxenites.

Clinopyroxene													
Rock type	Harz.	Harz.	Harz.	Harz.	Harz.	Harz.	Cpx. dike	Cpx. dike	Cpx. dike	Plag lherz.	Plag lherz.	Plag lherz.	Plag lherz.
Sample number	Fr12-48	Fr12-48	Fr12-48	Fr12-46	Fr12-46	Fr12-46	Fr12-53A	Fr12-53A	Fr12-53A	SZ11-143	SZ11-143	SZ11-143	SZ11-143
LA diameter spot	60	60	60	60	60	60	60	60	60	60	60	60	60
Concentration (ppm)													
Li	10.33	8.32	6.54	1.72	1.29	2.64	6.02	3.17	9.07	3.37	2.95	5.15	3.19
Sc	48.70	50.80	53.55	46.84	48.68	47.17	43.32	47.36	55.64	54.26	58.87	57.44	54.89
Ti	132	133	136	163	151	146	146	116	197	1908	1672	1830	1763
V	199	199	201	243	233	222	155	144	206	324	293	311	302
Cr	8756	8270	8103	11,008	8972	9219	4299	1799	4002	8650	6989	8408	8328
Co	24	26	25	28	26	25	40	29	40	25	24	24	28
Ni	407	410	403	425	440	406	503	299	487	394	362	373	421
Sr	0.69	0.85	1.05	0.04	0.02	0.63	4.71	12.02	4.56	0.09	0.15	1.89	0.09
Y	1.11	1.11	1.10	1.37	1.36	1.22	0.91	2.05	1.27	13.03	12.60	13.17	12.40
Zr	0.16	0.14	0.13	0.10	0.08	0.09	0.47	5.97	0.60	1.45	1.27	1.42	1.33
Nb	0.09	0.09	0.07	0.13	0.10	0.10	0.07	0.04	0.06	0.10	0.09	0.10	0.11
Ba	0.53	0.90	0.37	0.04		0.20	0.70	1.14	0.96			0.10	
La	0.007	0.007	0.010				0.207	0.793	0.113				
Ce	0.018	0.017	0.022				0.407	2.054	0.281	0.027	0.023	0.026	0.026
Pr	0.004	0.004	0.003				0.045	0.241	0.042	0.033	0.028	0.033	0.031
Nd		0.023					0.176	0.820	0.189	0.594	0.513	0.593	0.569
Sm							0.052	0.189	0.059	0.675	0.575	0.680	0.617
Eu	0.007	0.008	0.006				0.022	0.038	0.029	0.246	0.219	0.247	0.245
Gd	0.036	0.045	0.046	0.048	0.043	0.037	0.082	0.220	0.108	1.483	1.351	1.484	1.404
Tb	0.012	0.013	0.014	0.018	0.015	0.014	0.014	0.043	0.023	0.306	0.285	0.304	0.284
Dy	0.144	0.147	0.150	0.186	0.170	0.169	0.153	0.331	0.208	2.450	2.264	2.410	2.279
Ho	0.041	0.041	0.043	0.048	0.051	0.046	0.038	0.073	0.049	0.536	0.486	0.526	0.496
Er	0.161	0.154	0.163	0.219	0.185	0.180	0.118	0.251	0.151	1.558	1.440	1.533	1.450
Tm	0.024	0.028	0.026	0.042	0.034	0.027	0.018	0.039	0.024	0.219	0.192	0.209	0.199
Yb	0.202	0.196	0.229	0.268	0.269	0.236	0.140	0.299	0.192	1.410	1.314	1.355	1.324
Lu	0.032	0.033	0.037	0.043	0.041	0.034	0.023	0.044	0.031	0.185	0.170	0.175	0.168
Hf								0.17		0.24	0.21	0.21	0.23
Pb	0.12	0.21	0.19	0.11	0.08	0.07	0.33	0.32	0.18	0.05	0.12	0.07	0.09

Blank: data below the detection limit. na: not analyzed.

A second 1 ml HNO_3 was again added and evaporated to near dryness. Finally 2.5 ml HNO_3 was added and diluted to 50 ml after the addition of an internal standard giving a final concentration of 20 ppb Re and Rh. The internal standard was used to compensate for any analytical drift and matrix suppression effects. Calibration of the ICP-MS was via international rock standards (BHVO-1, AGV-1, W-2, and NBS688) with the addition of an in-house peridotite standard (GP13) (Ottley et al., 2003). These standards and analytical blanks were prepared by the same technique as the samples. To improve the signal-to-noise threshold for the low abundance isotopes, instrument dwell times were increased (Ottley et al., 2003). The composition of the reference samples (W-2, AGV-1, BHVO-1, BE-N, NBS688) was analyzed as an unknown during the same analytical runs. For the analyzed elements, reproducibility of these reference samples is generally better than 2% and the measured composition compares favorably with that published in Potts et al. (1992).

Major-element compositions of minerals from Sabzevar mantle peridotites were determined by JEOL wavelength dispersive electron probe X-ray micro-analyzer (JXA 8800R) at Kanazawa University. Accelerating voltage, beam current, and beam diameter for the analyses were 20 kV, 20 nA, and 3 μm, respectively. Representative mineral compositions are reported in Appendices 3 to 5. Trace-element abundances in clinopyroxenes (Table 2) in the examined peridotites were determined in-situ by LA-ICP-MS at Kanazawa University. Analyses were mainly performed by ablating 60-μm diameter spots on clinopyroxenes. All analyses were performed at 6 Hz with an energy density of 8 J/cm^2 per pulse. Calibration was carried out by analyzing NIST 612 glass as an external standard and 29Si as an internal standard based on SiO_2 concentration obtained by the electron microprobe. NIST 614 glass (secondary standard) was measured for quality control of each analysis. Precision or reproducibility is better than 5% for most elements, except Cr and Ni for which it is better than 10%. The accuracy and data quality based on the reference material (NIST 614) are high, as described by Morishita et al. (2005). Mg# is Mg / (Mg + total Fe) atomic ratio for silicates, and Mg / (Mg + Fe^{2+}) atomic ratio in chromian spinel, calculated assuming spinel stoichiometry. Cr# is Cr / (Cr + Al) atomic ratio.

5. Results

5.1. Whole rock major and trace element composition of Sabzevar peridotites

Representative whole rock compositions of Sabzevar mantle rocks are listed in Table 1. A more complete data set will be presented elsewhere. Sabzevar peridotites are variably serpentinized, evidenced by high LOI abundances (6.7–15.6 wt.%), except for wehrlitic dikes around the Gaft Chromitite Mine region (Table 1). Gaft and Forumad harzburgites as well as Baghjar-Kuh Siah harzburgite and dunites have high concentrations of MgO (44.4–50 wt.%, anhydrous basis) with low Al_2O_3 (0.02–0.9 wt.%) and CaO (0.12–1.2 wt.%) abundances, consistent with the presence of minor modal clinopyroxene, suggesting that these rocks are high degree partial melts of primitive mantle (Fig. 7), similar to SSZ peridotites. These rocks also have very low TiO_2 contents (Fig. 7). In contrast, the Baghjar-Kuh Siah lherzolites have higher CaO (2.4–2.5 wt.%) and Al_2O_3 (2.3–2.4 wt.%) (but lower TiO_2; 0.0007–0.001 wt.%; except two samples with ~0.04 TiO_2), and lower MgO (39.2–39.9 wt.%) abundances (Fig. 7), consistent with the presence of modal clinopyroxene and plagioclase.

The Baghjar-Kuh Siah dunites are characterized by highly depleted REE patterns, with continuous depletion from Lu toward Dy and slight

Plag lherz.	Plag lherz.	Plag lherz.	Plag lherz.	Weh. dike	Weh. dike	Weh. dike	Weh. dike	Harz.	Harz.	Harz.	Harz.			
SZ11-127	SZ11-127	SZ11-127	SZ11-127	GA12-3	GA12-3	GA12-3	GA12-3	GF12-3	GF12-3	GF12-3	GF12-3	Typical detection limit		
60	60	60	60	50	50	50	50	40	40	40	40	60	50	40
3.43	3.33	3.04	3.21	4.66	3.80	3.88	4.44	5.51	8.30	3.87	5.82	0.1495	0.487	0.701
58.28	64.10	61.40	56.62	na	na	na	na	na	na	na	na	0.0498	na	na
1554	1672	1660	1622	492	557	594	621	455	525	551	510	0.1943	0.350	0.655
313	320	323	315	na	na	na	na	na	na	na	na	0.0355	na	na
8391	8239	7910	7778	na	na	na	na	na	na	na	na	1.6388	0.063	0.118
26	23	25	23	na	na	na	na	na	na	na	na	0.0145	na	na
405	369	391	377	na	na	na	na	na	na	na	na	0.6360	na	na
0.14	0.09	0.11	0.15	5.45	5.79	6.16	6.24	8.57	9.30	7.11	7.76	0.0057	0.006	0.019
12.42	12.77	12.84	12.49	2.29	2.59	2.72	2.87	2.46	2.61	3.09	2.67	0.0051	0.000	0.007
1.38	1.45	1.42	1.40	0.52	0.72	0.79	0.80	1.28	1.45	1.77	1.51	0.0094	0.006	0.014
0.10	0.10	0.10	0.10	0.03	0.02	0.02	0.02	0.01	0.02	0.03	0.03	0.0055	0.007	0.008
					0.09	0.35	0.11	0.34	2.61	1.21	0.42	0.0353	0.019	0.039
				0.032	0.035	0.036	0.034	0.035	0.034	0.031	0.033	0.0036	0.005	0.017
0.026	0.027	0.028	0.029	0.148	0.157	0.173	0.169	0.168	0.161	0.153	0.155	0.0029	0.003	0.005
0.034	0.033	0.034	0.031	0.032	0.038	0.037	0.045	0.041	0.038	0.036	0.036	0.0028	0.005	0.010
0.556	0.562	0.567	0.569	0.259	0.277	0.323	0.311	0.315	0.292	0.310	0.292	0.0168	0.015	0.034
0.610	0.634	0.642	0.633	0.136	0.164	0.170	0.188	0.198	0.193	0.208	0.191	0.0202	0.020	0.026
0.261	0.253	0.254	0.261	0.064	0.072	0.079	0.079	0.091	0.077	0.077	0.071	0.0058	0.007	0.014
1.379	1.375	1.393	1.391	0.269	0.335	0.357	0.360	0.361	0.365	0.418	0.388	0.0229	0.028	0.038
0.280	0.290	0.279	0.286	0.049	0.064	0.063	0.068	0.068	0.071	0.081	0.070	0.0050	0.006	0.009
2.237	2.230	2.196	2.298	0.429	0.493	0.513	0.546	0.513	0.519	0.620	0.563	0.0146	0.012	0.044
0.477	0.482	0.492	0.492	0.089	0.106	0.118	0.115	0.105	0.106	0.128	0.113	0.0052	0.004	0.010
1.395	1.435	1.374	1.423	0.273	0.294	0.330	0.342	0.285	0.289	0.356	0.303	0.0108	0.010	0.017
0.192	0.205	0.197	0.199	0.038	0.046	0.045	0.046	0.038	0.041	0.052	0.045	0.0052	0.005	0.005
1.296	1.354	1.286	1.328	0.279	0.325	0.327	0.350	0.248	0.272	0.320	0.275	0.0176	0.019	0.028
0.173	0.182	0.171	0.177	0.040	0.043	0.043	0.054	0.033	0.038	0.045	0.038	0.0039	0.006	0.011
0.18	0.18	0.20	0.21	0.02	0.03	0.04	0.05	0.10	0.11	0.14	0.12	0.0197	0.020	0.028
	0.06	0.10	0.11	0.15	0.07	0.12	0.12	0.11	0.79	0.10	0.03	0.0456	0.057	0.098

LREE enrichment (Fig. 8). Harzburgite from this region has higher bulk REE content but is REE-depleted (Fig. 8). Baghjar-Kuh Siah lherzolites have higher bulk REE content but with depletion from Sm to La, resembling abyssal peridotites (Niu et al., 1997). In addition all rocks show pronounced peaks in Th, Nb (except lherzolites), Zr (except dunites), Y (except lherzolites), Sr and Pb (Fig. 8).

Forumad harzburgites have depleted bulk REE content with steep trend from Lu to Gd, similar to forearc residues (Fig. 8). Gaft harzburgites are similar to Forumad harzburgites with depletion in all REEs and steep patterns from Lu to Gd, showing residues after a high degree of partial melting. All of these samples show enriched peak in U, Sr, and Pb and negative anomalies in Nb and Y. Gaft wehrlite is slightly enriched in LREEs relative to HREEs, with depletion in Nb–Sr and enrichment in Th, U, and Pb resembling calc-alkaline rocks.

5.2. Major element composition of chromitite and peridotite minerals

5.2.1. Baghjar-Kuh Siah peridotite massif

Baghjar-Kuh Siah plagioclase lherzolites contain olivines with 90.2 to 90.7 forsterite (Fo) (Fig. 9; Appendix 3A). Harzburgite olivines show higher Fo content ranging from 90.8 to 91.8 whereas dunite olivines show even higher Fo content, 91.7 to 92.8 (Fig. 9). Olivines are more magnesian in podiform chromitite than in mantle peridotites (Fo = 93.4 to 96.3). Their high Mg content reflects re-equilibration with spinels by subsolidus Mg–Fe^{2+} re-equilibration (Arai, 1980). The NiO content is quite high in chromitite olivines, from 0.5 to 0.7 wt.%, higher than in peridotite olivines (0.2–0.4 wt.%, Fig. 9; Appendix 3A). Like olivines, orthopyroxenes have high Mg#, ~0.90–0.91 in plagioclase lherzolite and 0.91–0.92 in harzburgite, but the clinopyroxenite orthopyroxene shows lower Mg#, 0.86 (Appendix 3D). Orthopyroxenes show higher Al_2O_3 (2.7–4.9 wt.%) in plagioclase lherzolite than in harzburgites (1.5–3 wt.%) (Fig. 10B). Plagioclase lherzolites also contain aluminous clinopyroxene (3.1–5.9 wt.% Al_2O_3) compared to harzburgite (2–3.4 wt.% Al_2O_3) (Fig. 10A). Clinopyroxenites contain low-Al (0.4 t 1.1 wt.% Al_2O_3; Appendix 3C) clinopyroxenes. Compared to harzburgites, the Baghjar-Kuh Siah plagioclase lherzolites contain clinopyroxene with high content of TiO_2 (0.22–0.34 wt.%) and Na_2O (0.35–0.51 wt.%) (Fig. 10C). Spinels associated with lherzolite clinopyroxenes have low Cr#, ranging from 0.13 to 0.36 (Appendix 3B) (Fig. 11). Residual spinels from harzburgites are characterized by medium Cr# (0.34–0.45) whereas dunites have higher Cr# spinels (0.65–0.71) (Appendix 3B; Fig. 11). Harzburgite spinels are commonly similar in Cr# to typical MOR spinels and could be residues after low degrees of melting (12–16%) (Fig. 11C). Chromian spinels from podiform chromitites show distinctive compositions; occupying the boninitic field in Cr# vs. Mg# diagram (Fig. 11A).

5.2.2. Gaft Chromitite Mine peridotite massif

Olivines in Gaft Chromitite Mine harzburgites show $Fo_{91.2–91.7}$ while dunite olivines have slightly higher Fo contents, 91.1–92.4 (Appendix 4A). Their NiO content varies between 0.34 and 0.41%, typical of mantle olivines (Takahashi, 1980). Harzburgites have similar olivine compositions to other refractory harzburgites from Sabzevar peridotite massifs (Fig. 9). Wehrlites contain olivines with lower Fo (~86) and NiO (0.09–0.15 wt.%) contents. The Fo content of olivine can be lowered in clinopyroxene-rich rocks by re-equilibration with surrounding phases during subsolidus cooling (e.g., Obata et al., 1974; Loucks, 1996). Harzburgite orthopyroxenes have high Mg# (~0.92) and low Al_2O_3 content (0.84–1.8 wt.%; Appendix 4C). Dunites contain orthopyroxenes with higher Mg# (~0.93) and lower Al_2O_3 (0.7–0.9 wt.%) compared to

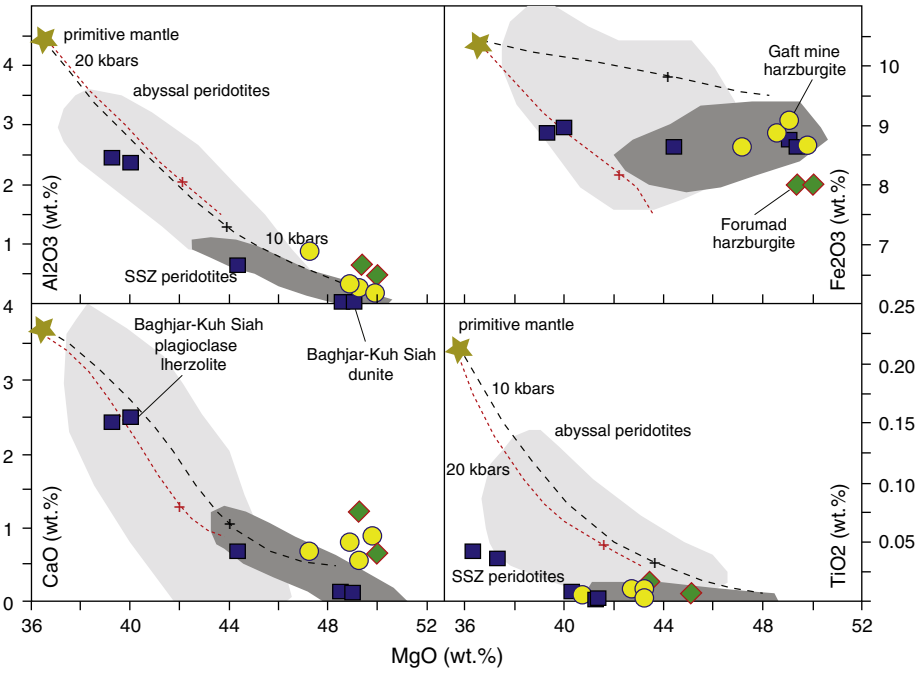

Fig. 7. Variation diagrams of MgO vs. selected major elements (anhydrous, volatile-free) in bulk rock peridotites from the Sabzevar peridotites. Abyssal and SSZ peridotites fields are from Niu et al. (1997) and Parkinson and Pearce (1998) respectively. Melting trends at 10 and 20 kbar of primitive mantle are from Ghiorso et al. (2002). Tick marks on melting curves display clinopyroxene disappearance.

harzburgites (Fig. 10B). Relict clinopyroxenes from harzburgites and dunites mostly show low Al_2O_3 content (<1%), but some grains have >1% Al_2O_3, and probably crystallized from wehrlitic melts as dike/veins passed through and interacted with the host harzburgite/dunite. These clinopyroxenes contain higher TiO_2 and Na_2O (Fig. 10C). Clinopyroxene from wehrlitic dikes shows bimodal distributions of Mg#, Al_2O_3 and TiO_2 abundances (Fig. 10). The Na_2O and TiO_2 abundances of these clinopyroxenes are lower than those in equilibrium with MORB (Fig. 10C). Harzburgite spinels show high Cr# (~0.53 to 0.68) along with low TiO_2 (<0.15%) (Fig. 11A and B). This spinel Cr# is commonly higher than those of typical MOR spinels, and could be a residue after high degrees of partial melting of mantle harzburgite. Dunite spinels are commonly characterized by higher Cr# (0.58–0.77) but show similar TiO_2 abundance (0.05–0.36 wt.%) compared to harzburgite spinels. The composition of low Cr# spinel in the dunite resembles that from depleted harzburgite (Fig. 11A). Chromian spinel in the podiform chromitites show bimodal Cr#: 0.77–0.78 (high Cr# varieties) and 0.41–0.43 (low Cr# varieties). The former chromitite has massive texture, and are crosscut by wehrlitic dikes whereas the latter has nodular texture and are cut by gabbroic dikes. Low Cr# chromitite commonly has higher TiO_2 content (0.19–0.29%) compared to high Cr# chromitite (0.13–0.23%). Fine-grained magmatic spinels from wehrlitic dikes are Fe- and Ti-rich (>24% FeO and >0.17 TiO_2; Appendix 4B) with low Mg# (0.26–0.48) (Fig. 11).

5.2.3. Forumad chromitite–peridotite massif

Harzburgite olivines show relatively constant Fo contents (91.5–91.8) whereas olivine in podiform chromitite is highly magnesian ($Fo_{95.6–97.4}$), again suggesting that olivine geochemistry has been modified during subsolidus $Mg–Fe^{2+}$ cation exchange (Arai, 1980). NiO content of harzburgite olivines is similar to that of other Sabzevar peridotites (0.37–0.40%, Appendix 5A) while NiO content of chromitite olivines is

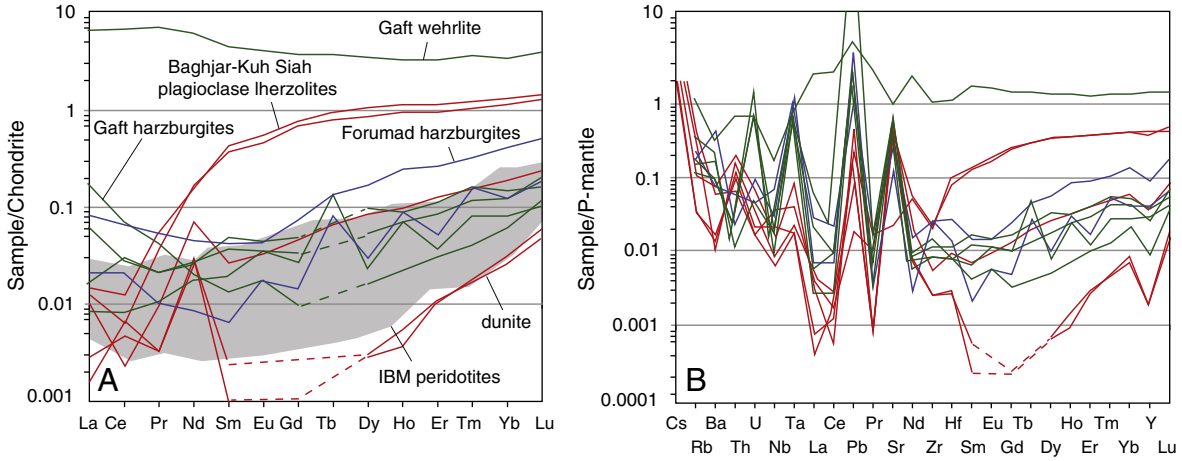

Fig. 8. Chondrite and primitive mantle-normalized REE and multi-element diagrams for Sabzevar mantle rocks. Chondrite normalization values are from Sun and McDonough (1989). The composition of Izu–Bonin–Mariana (IBM) forearc peridotites is from Parkinson and Pearce (1998).

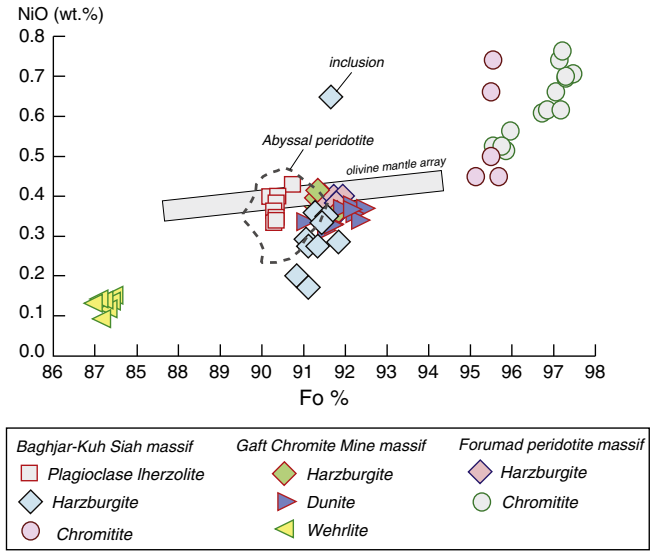

Fig. 9. NiO versus forsterite content of olivine grains from the Baghjar-Kuh Siah, Gaft Chromitite Mine and Forumad mantle peridotites, chromitites and wehrlites. Field for olivine mantle array is after Takahashi et al. (1987).

higher than 0.5 wt.% (Fig. 9). Harzburgite orthopyroxene has low Al_2O_3 contents (1.6–1.9 wt.%, Appendix 5C), slightly higher than Gaft Chromitite Mine harzburgite orthopyroxenes but lower than those of Baghjar-Kuh Siah harzburgite. Clinopyroxene has Mg# and Al_2O_3 ranging from 0.93 to 0.96 and 0.7 to 3.5 wt.% (Appendix 5D). Clinopyroxenites have clinopyroxene with lower Mg# (~0.90–0.92) and Al_2O_3 (0.3–1.3 wt.%) (Fig. 10A). Clinopyroxene in harzburgites is subdivided into two types: 1) clinopyroxene with low TiO_2 and Na_2O abundances and 2) clinopyroxene with higher TiO_2 and Na_2O contents (Fig. 10C). This geochemical behavior is independent of clinopyroxene Al_2O_3 content, as the varieties with high Al content have lower Ti and Na abundances (Appendix 5D). Spinel in harzburgite exhibits a bimodal Cr#, higher in harzburgites (~0.56) and lower in clinopyroxene-bearing harzburgites (0.42–0.49) (Appendix 5B). These spinels have similar TiO_2 abundances (Fig. 11B). Forumad podiform chromitites define two groups: 1) inclusion-free and high Cr# chromian spinels (Cr# 0.77–0.83) and 2) inclusion-bearing (clinopyroxene and/or tremolite), low Cr# (0.65–0.66) and higher TiO_2 (~0.2 wt.%) spinels (Appendix 5B).

5.3. Trace element composition of peridotite clinopyroxene

Trace element (including REE) abundances in Sabzevar ultramafic rock clinopyroxenes, including the Baghjar-Kuh Siah plagioclase

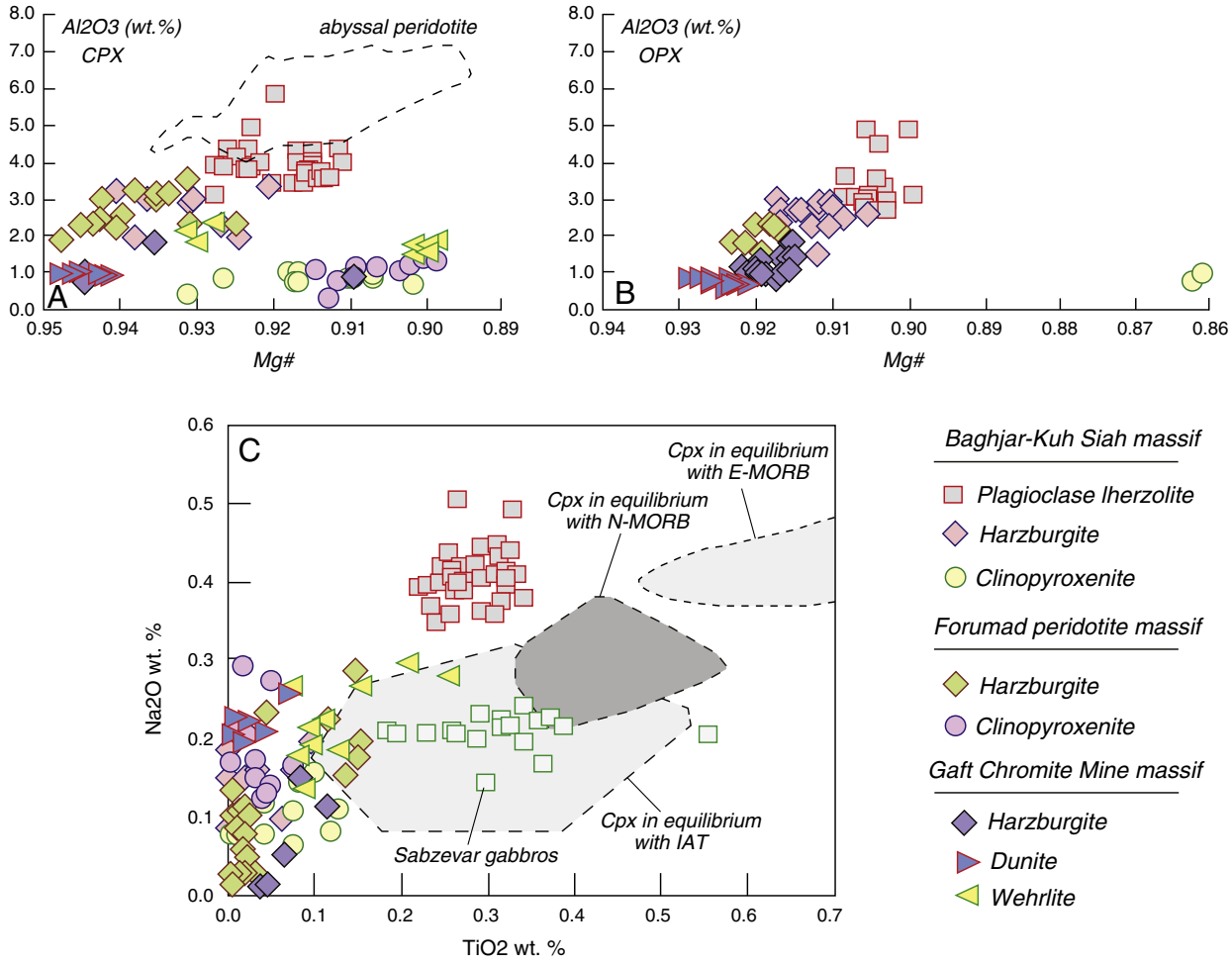

Fig. 10. A) Al_2O_3 against Mg# for clinopyroxene, B) Al_2O_3 versus Mg# for orthopyroxene and C) Na_2O versus TiO_2 for clinopyroxene (modified after Akizawa et al., 2012) from the Baghjar-Kuh Siah, Gaft Chromitite Mine and Forumad mantle peridotites, chromitites and pyroxenites. Clinopyroxene in equilibrium with island-arc tholeiitic (IAT) lavas is based on the clinopyroxene data on the arc tholeiitic pillow lavas of the Nain ophiolite, Central Iran (Shafaii Moghadam, 2009). Data on Sabzevar gabbros are from Shafaii Moghadam et al. (unpublished data).

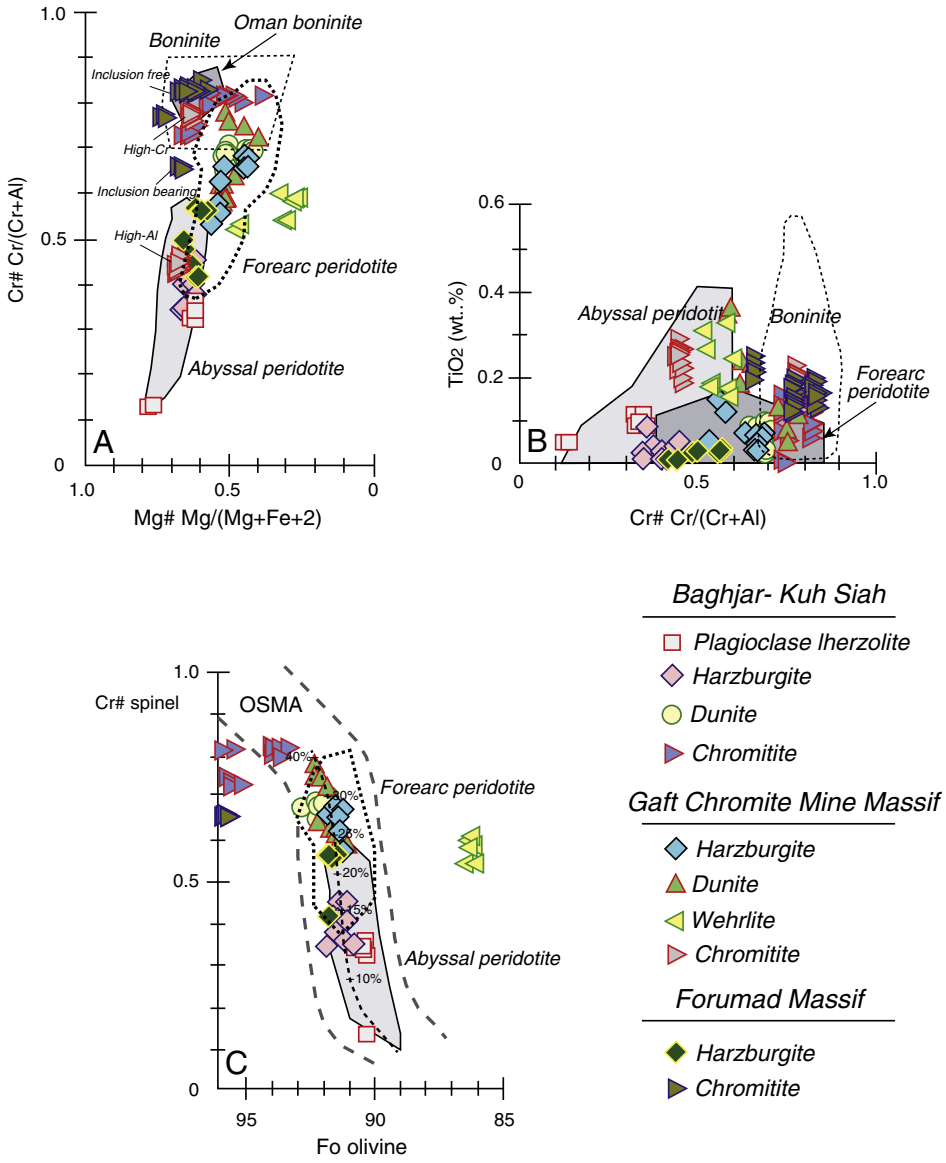

Fig. 11. A) Compositional variations of chromian spinels of chromitite pods and host peridotites/intrusive wehrlites from the Baghjar-Kuh Siah, Gaft Chromitite Mine and Forumad peridotite massifs in (A) Cr# vs. Mg# (modified after Dick and Bullen, 1984), (B) TiO_2 vs. Cr# (after Tamura and Arai, 2006) and (C) olivine Fo vs. spinel Cr# (Arai, 1994) diagrams.

lherzolite, the Forumad harzburgite and clinopyroxenite and the Gaft Chromitite Mine wehrlite and harzburgite, are listed in Table 2; REE and extended trace element patterns are shown in Fig. 12. All Sabzevar ultramafic rocks studied here show important similarities: 1) all but Forumad clinopyroxenites show strong LREE and Zr depletion; 2) Sr may be enriched or depleted; and 3) all are Ti-depleted. Chondrite-normalized REE patterns of clinopyroxenes from the melt-pocket domains of Baghjar-Kuh Siah plagioclase lherzolites are strongly depleted in the light and middle REEs (LREE–MREE; Fig. 12A). Clinopyroxenes are depleted in Ti, Zr and Sr (Fig. 12B); the Sr depletion may be due to plagioclase crystallization. HREE abundances in clinopyroxene range between six and eight times those of chondrite and are similar to those in Sabzevar cumulate gabbros, although the extent of LREE depletion is greater (Fig. 12A). On a N-MORB normalized diagram, the melts calculated to be in equilibrium with Baghjar-Kuh Siah plagioclase lherzolite clinopyroxenes show LREE depletion and negative Sr, Zr, and Ti anomalies (Fig. 13). Although the extent of HREE enrichment in equilibrated melts is similar to that in MORB-like forearc basalts (FAB) of Reagan et al. (2010), depletion in LREE, Ti and Zr is more conspicuous (Fig. 13A). Clinopyroxene in Gaft Chromitite Mine harzburgite exhibits different REE patterns, similar to clinopyroxene from Sabzevar cumulate gabbros but with lower total REE contents (Fig. 12E). Although clinopyroxenes show depleted HREE, LREE abundances are greater than those in the plagioclase lherzolite clinopyroxenes. The Gaft harzburgite clinopyroxene is similar in REE patterns to clinopyroxene from MOR cumulates (Fig. 12E; Ross and Elthon, 1993), but shows more convex-upward patterns with Tb–Dy apices. Depletion in Zr and Ti and enrichment in Sr are more conspicuous (Fig. 12F). The REE abundances and patterns of clinopyroxenes in the Gaft Chromitite Mine wehrlitic dikes are also similar to those of MOR cumulates (Ross and Elthon, 1993) (Fig. 12C). They are similar to clinopyroxene patterns from Sabzevar cumulate gabbros but with lower REE abundances (Fig. 12C). Thus, clinopyroxene REE patterns from the Gaft Chromitite Mine harzburgites are similar to those of wehrlitic clinopyroxenes. Residual Cpxs (not impregnated) from Forumad harzburgites are depleted in REEs and show strongly LREE-depleted patterns, similar to those of supra-subduction zone peridotites (Fig. 12G). Clinopyroxenes in clinopyroxenite dikes, crosscutting the Forumad chromitites, show distinct REE and trace element patterns (Fig. 12G and H), with concave-upward patterns showing LREE enrichment. The melts calculated to be in equilibrium with these clinopyroxenes show U-shaped REE patterns similar to those of boninitic melts (Fig. 13A).

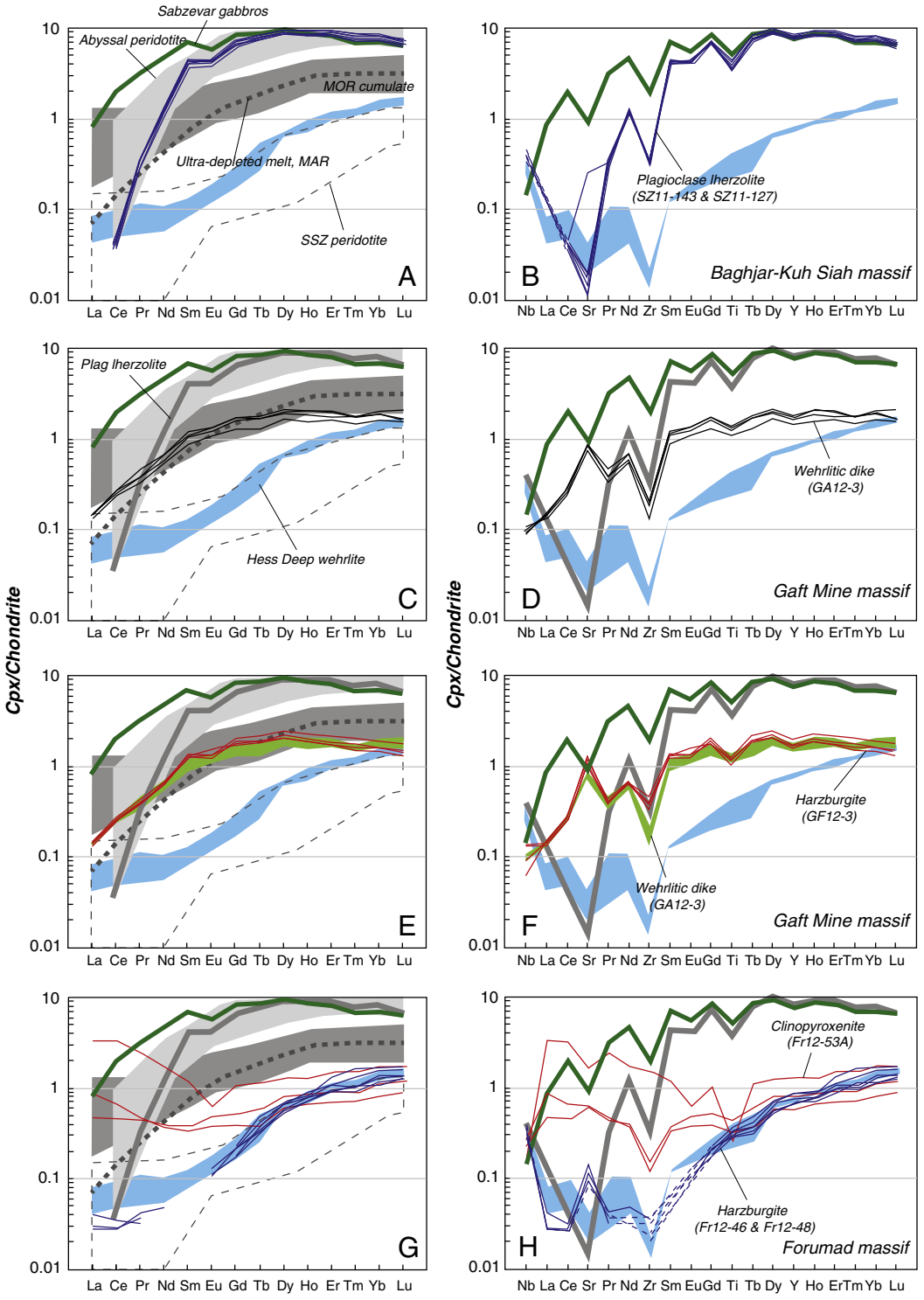

Fig. 12. Rare earth and trace element abundances of clinopyroxene in peridotites, wehrlites and clinopyroxenites from the Baghjar-Kuh Siah plagioclase lherzolite (A, B), Gaft Chromitite Mine wehrlite dikes (C, D), Gaft Chromitite Mine harzburgites (E, F), and Forumad harzburgite and clinopyroxenite (G, H) massifs. Chondrite normalization values are from Sun and McDonough (1989). Fields for abyssal and supra-subduction zone (SSZ) peridotites clinopyroxene are from Johnson and Dick (1992) and Johnson et al. (1990). The composition of ultra-depleted melt from the Mid-Atlantic Ridge (MAR) is from Sobolev and Shimizu (1993), and the field for MOR cumulate Cpx is from Ross and Elthon (1993). Data on Sabzevar gabbro clinopyroxene is from Shafaii Moghadam et al. (unpublished data). Clinopyroxenes from Hess Deep wehrlites are from Arai and Takemoto (2007).

6. Discussion

6.1. SSZ versus MORB tectonic setting

Detailed discussion of the Sabzevar ophiolite and its tectono-magmatic setting in the context of whole rock geochemical data of lavas and peridotites is beyond the scope of this study and will be presented elsewhere. Although the ophiolite has not been studied in detail, our unpublished data together with scarce published data (e.g., Shojaat et al., 2003; Maleki, 2013) show that calc-alkaline and arc tholeiitic lavas (with high LILE/HFSE, similar to arc lavas) are dominant in the Sabzevar ophiolite crustal section. Cumulates, locally layered gabbros, gabbronorites and hornblende gabbros with depleted signatures of boninitic affinity are abundant in the Sabzevar crustal section.

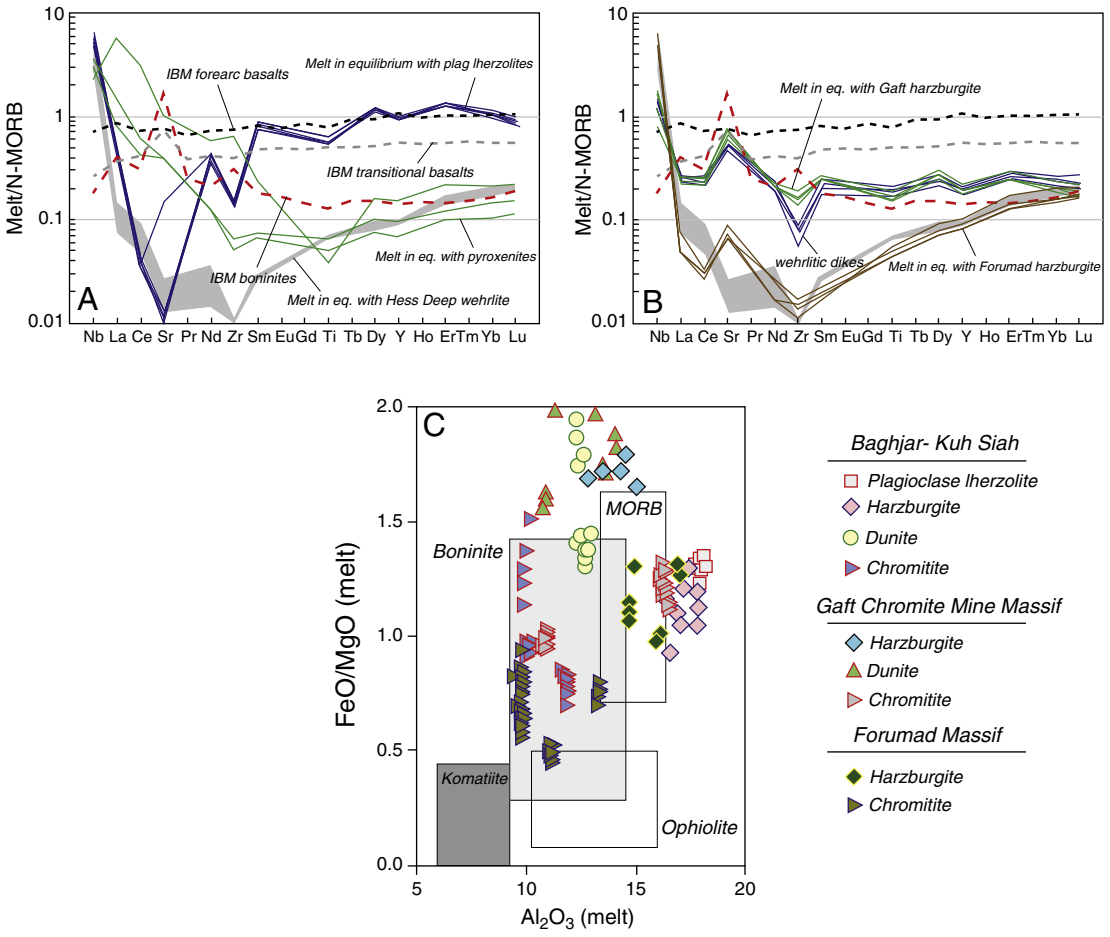

Fig. 13. Calculated melts in equilibrium with clinopyroxene (using D's from Hart and Dunn, 1993) for Baghjar-Kuh Siah plagioclase lherzolites (A) and Forumad clinopyroxenites and from Gaft mine harzburgites and wehrlitic dikes (B), normalized relative to N-MORB values (N-MORB data from Sun and McDonough, 1989). Izu–Bonin–Mariana forearc and transitional basalts and boninites (Reagan et al., 2010) are shown for comparison. Clinopyroxenes from Hess Deep wehrlites are from Arai and Takemoto (2007). C — Parental melt composition in equilibrium with the Sabzevar chromian spinels in terms of $(FeO/MgO)_{melt}$ vs. $(Al_2O_3)_{melt}$ (wt.%) using Maurel and Maurel (1982) calculation (modified after Merlini et al., 2011).

These gabbros show very low trace-element and REE abundances and are characterized by high εNd, confirming a depleted mantle source (Shafaii Moghadam et al., unpublished data). These observations highlight a supra-subduction zone setting for the formation of the Sabzevar ophiolites. Bulk trace elements data show that the Sabzevar mantle harzburgites (except impregnated lherzolites) are residues after high degree of partial melting similar to peridotites from the IBM forearc region (Parkinson and Pearce, 1998). Most harzburgite spinels (except those crystallized from infiltrating MORB-like wehrlites) show medium to high Cr# (>0.5) along with low TiO_2 contents, similar to those from arc harzburgites (Fig. 11). Mantle peridotites from supra-subduction zone environments are characterized by depleted harzburgite, containing spinels mostly with Cr# >0.50 and low TiO_2 contents (Bloomer and Hawkins, 1983; Parkinson and Pearce, 1998; Stern, 2010). In the olivine Fo versus spinel Cr# diagram, the Gaft Chromitite Mine harzburgites are residues after >25% partial melting, whereas the Forumad harzburgites reflect variable degrees of partial melting of fertile peridotite <15% (clinopyroxene-bearing harzburgite) and >22% (harzburgite) (Fig. 11C). The calculated average degree of partial melting producing the abyssal peridotites was suggested to be 10–20% using spinel geochemistry (Kamenetsky et al., 2001). Sabzevar chromitites are also characterized by high Cr#, excepting the nodular chromitites at the Gaft Chromitite Mine, and were probably formed from a boninitic melt. Such high-Cr# chromitites are not reported from normal ocean floor peridotites, but are common from arc-related environments (e.g., Arai and Abe, 1994; Arai, 1997a, 1997b). These geochemical signatures for the Sabzevar ophiolite, from mantle rocks to the overlying crustal magmatic units, suggest a supra-subduction zone for the genesis and evolution of the ophiolite.

6.2. Residual versus impregnating/magmatic clinopyroxenes: evidence of hydrous melting, refertilization and arc magmatism

Complex magma behavior in the upper mantle section and at MTZ's has been investigated in ophiolitic as well as in oceanic abyssal peridotites (e.g., Kelemen et al., 1995; Sano and Kimura, 2007; Tamura et al., 2008; Aldanmaz et al., 2009; Uysal et al., 2012). These observations emphasize that variable compositions of mantle rocks from different tectonic environments reflect different styles of depletion and refertilization (Kelemen et al., 1997; Bizimis et al., 2000; Aldanmaz et al., 2012). In this context, the distribution of trace elements and REE in primary mantle clinopyroxenes may provide useful information on mantle depletion due to melt extraction and/or by metasomatism or impregnation (Johnson et al., 1990; Hellebrand et al., 2001, 2002). Melt impregnation in particular results in precipitation of secondary clinopyroxenes during infiltration of ascending magmas (Hellebrand et al., 2005).

Based on modal composition and bulk rock-mineral geochemistry, the Forumad harzburgites show a residual signature. Trace element and REE patterns of Forumad harzburgite Cpxs are similar to those of SSZ peridotites: both reveal a highly refractory nature (Fig. 12G, H). Steep slopes from HREE–MREE in clinopyroxene REE patterns have been reported from abyssal peridotites (e.g., Johnson et al., 1990; Hellebrand et al., 2002; Tamura et al., 2008). Such patterns in abyssal

peridotites were suggested to be produced during polybaric non-modal fractional melting, which operated initially in the garnet field and subsequently continued in the spinel lherzolite field (Johnson et al., 1990).

Strong LREE and MREE depletion in Forumad harzburgite clinopyroxenes suggests that they are residual after two-stage fractional melting, i.e., anhydrous early melting perhaps during subduction initiation, followed by hydrous melting triggered by fluids liberated from the subducting slab. The observed ultra-depleted LREE patterns (Fig. 12G) cannot be explained by simple spinel peridotite melting. In Ti versus Zr and Ti versus Dy diagrams (Bizimis et al., 2000) (Fig. 14), the clinopyroxenes show low Ti, Dy and Zr contents and are compositionally similar to clinopyroxenes in depleted SSZ harzburgites. These clinopyroxenes follow the hydrous partial melting trend (Bizimis et al., 2000).

The petrological characteristics of Baghjar-Kuh Siah plagioclase-bearing lherzolites are similar to those of oceanic and ophiolitic plagioclase peridotites (e.g., Seyler and Bonatti, 1997; Dijkstra et al., 2001; Sano and Kimura, 2007). Clinopyroxene composition of the Baghjar-Kuh Siah plagioclase lherzolites is distinct from that in other Sabzevar peridotites by having higher Na_2O, TiO_2 and REE abundances. Their REE patterns are similar to those of oceanic abyssal peridotite clinopyroxenes (Johnson et al., 1990; Johnson and Dick, 1992), but MREE enrichment is greater. Refertilization of peridotites by entrapped melts accounts for high Na_2O and TiO_2 contents in abyssal peridotites

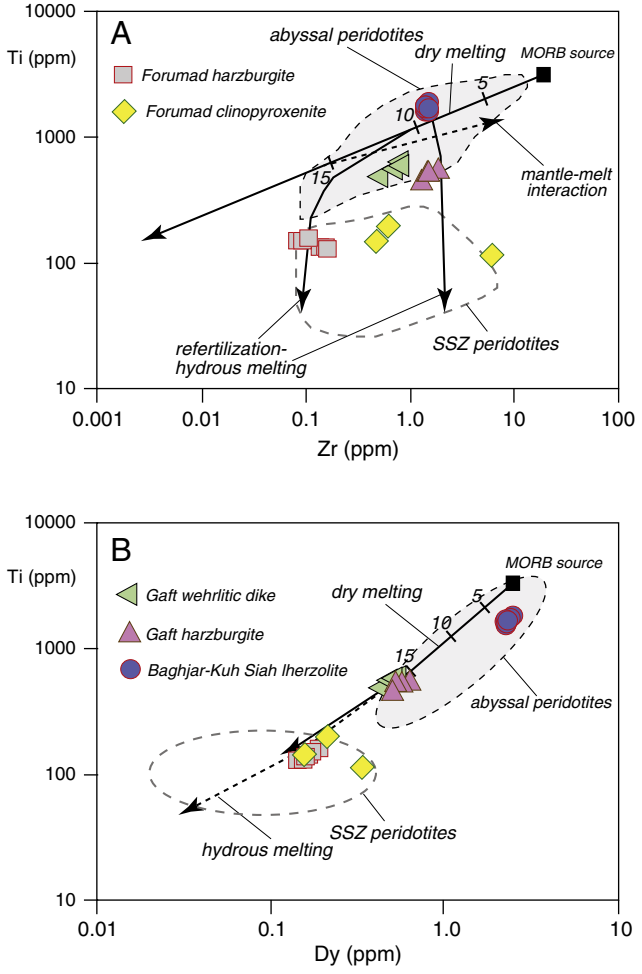

Fig. 14. Partial melting model for the Sabzevar peridotite based on the Ti vs. Zr (ppm) (A) and Ti vs. Dy (ppm) (B) in clinopyroxene. Dry melting is for residual clinopyroxene compositions in a MORB source and hydrous melting is the presence of fluids (modified after Bizimis et al., 2000). Fields for clinopyroxene in supra-subduction zone (SSZ; Bizmis Bizimis et al., 2000) and in abyssal peridotites (Johnson et al., 1990; Johnson and Dick, 1992) are used for comparison.

(Dick, 1989; Elthon, 1992; Seyler and Bonatti, 1997; Hellebrand et al., 2002; Piccardo et al., 2007; Tamura et al., 2008). The Baghjar-Kuh Siah lherzolite clinopyroxenes have high Zr and Dy (as well Ti) abundances, resembling fertile abyssal peridotites in the Ti vs. Dy and Zr diagram (Bizimis et al., 2000) (Fig. 14). Interaction between MORB-like magma and wall harzburgites could be responsible for high Mg# characteristics of clinopyroxenes in plagioclase lherzolites (Akizawa et al., 2012). Abundances of modal clinopyroxene and plagioclase (in melt pocket-shaped domains) in the Baghjar-Kuh Siah lherzolites suggests melt refertilization of residual peridotite. Crystallization of plagioclase is a further evidence of refertilized harzburgites.

Relatively high REE, especially LREE, abundances in clinopyroxene in the Gaft Chromitite Mine harzburgites, as well as the similarity of the REE patterns of clinopyroxene to wehrlitic dikes and the Sabzevar cumulate gabbros, may be caused by infiltration of small melt fractions. This infiltration may be similar to that generating clinopyroxene in the mantle section near the wehrlitic dikes. The harzburgite clinopyroxenes overlap with those of wehrlitic dikes in Ti vs. Dy and Zr diagrams (Bizimis et al., 2000) (Fig. 14), supporting the idea that these crystallized during impregnation by wehrlitic dike injection. The melts calculated to be in equilibrium with clinopyroxene from the Gaft Chromitite Mine wehrlitic dike and harzburgite show very depleted U-shaped REE patterns (with enrichment in LREE), resembling boninitic melts common in fore-arc environments such as those of IBM (e.g., Ishii et al., 1992; Stern and Bloomer, 1992; Pearce and Parkinson, 1993; Pearce and Parkinson, 1998; Stern, 2004) (Fig. 13B). The late intrusive wehrlites are common in the Oman MTZ (Uesugi et al., 2003). These rocks are also reported from the layered gabbros to beneath the sheeted dike complex (e.g., Benn et al., 1988; Koga et al., 2001; Koepke et al., 2009). The Na_2O and TiO_2 abundances of wehrlitic dike clinopyroxenes are lower than those in equilibrium with MORB and are more similar to clinopyroxene in equilibrium with depleted arc melts (Fig. 10C). The melt in equilibrium with magmatic clinopyroxenes from the Gaft Chromitite Mine wehrlites is depleted, but is different from the melt in equilibrium with Hess Deep wehrlite clinopyroxenes. These clinopyroxenes follow the mantle–melt interaction trend (Fig. 14A).

6.3. High Cr# versus low Cr# chromitites: different melt compositions?

Podiform chromitites occur mainly in ophiolites and their genesis is thought to reflect melt/rock interaction in the upper mantle (e.g., Zhou and Robinson, 1994; Arai et al., 1997; Zhou and Robinson, 1997). The compositional diversity of chromitites in terms of their Cr content is a common feature of many ophiolites and is attributed to different magma compositions (Ahmed et al., 2012). High Cr# podiform chromitites are thought to be crystallized from boninitic melts in an arc-related environment and low Cr# chromitites from MORB-like (probably FAB-like magma) tholeiitic magma during melt/mantle interaction. The low Cr# chromitites are also suggested to form in the mantle beneath back-arc basins (e.g., Zhou and Robinson, 1997; Zhou et al., 1998). There is a general consensus for the formation of podiform chromitites including multistage melting, melt segregation and magma mixing within magma conduits in the upper mantle (Paktunc, 1990; Leblanc and Ceuleneer, 1992; Shi et al., 2012); and/or melt–rock interaction and its subsequent mixing (Zhou et al., 1994; Arai and Yurimuto, 1995; Zhou et al., 1996; Arai et al., 1997; Zhou and Robinson, 1997). During continuous melt percolation in arc-related mantle, dunitic residues can form as pyroxenes from host peridotites are dissolved into the percolating melts and Cr concentrates into these melts (Dick and Bullen, 1984). Thus this modified melt could crystallize chromitite (Arai and Yurimoto, 1994). The melt/mantle interaction can produce a secondary melt which is enriched in Si and Cr by selective dissolution of host peridotite orthopyroxenes (Arai and Yurimoto, 1994; Arai, 1997a). Mixing of this Si- and Cr-rich magma with subsequent primitive and spinel under-saturated melts would precipitate chromian spinel (Arai, 1997b). The presence or absence of podiform chromitites in

ophiolites as well as their compositional varieties is initially dependent on the host peridotite lithology and the composition of interacting melts (Arai, 1997a, 1997b; Ahmed et al., 2012). The podiform chromitites are mainly hosted by moderately refractory harzburgites with intermediate spinel Cr# ranging from 04 to 0.6 (Arai, 1997a, 1997b).

Two types of chromitite pods occur in the mantle section of the Sabzevar ophiolite. Although low Cr# podiform chromitites are less common than high Cr# pods, their occurrence is important. The chromian spinel from the Gaft mine low Cr# podiform chromitites has relatively high Al_2O_3 (~29–31 wt.%) with Cr# (0.43–0.46) similar to MORB-related spinels (Cr# = 20–54) (Dick and Bullen, 1984; Zhou et al., 2001). The TiO_2 content of spinels in Gaft chromitites is also relatively high (0.2–0.3 wt.%), again similar to MORB-related spinels. Such low Cr# podiform chromitites are associated with troctolitic and gabbroic dikes (Zhou et al., 2001). Low Cr# chromitites are thought to be crystallized from a MORB-like tholeiitic melt while high Cr# chromitite pods were probably formed from a depleted melt with boninitic geochemical signature (Zhou and Robinson, 1994, 1997; Zhou et al., 1998, 2001). Around the Gaft Chromitite Mine, gabbroic dikes crosscut the low Cr# nodular chromitites, but the dikes are narrow (5 to max 30 cm wide) and troctolitic dikes are missing. Other Sabzevar ophiolite chromitite pods are high Cr# and are believed to have crystallized from high-Mg boninitic melts. The exception is some pods from the Forumad region with inclusion-rich chromian spinels that contain slightly lower Cr# than other podiform high Cr# chromitites. Podiform chromitites with high Cr# spinels seem to have formed from a boninitic melt whereas those with low Cr# are thought to have originated from a hydrous, depleted tholeiitic melt.

The FeO, MgO and Al_2O_3 contents of chromian spinels in podiform chromitites is considered to be the function of melt composition from which they formed (e.g., Maurel and Maurel, 1982; Kamenetsky et al., 2001). The Al_2O_3 content of parental melts in equilibrium with Sabzevar high Cr# chromitites, calculated using Maurel and Maurel (1982) equation, is <13.3 wt.%, entirely in the range of boninitic magma composition in arc setting (Al_2O_3 = 10.6–14.4 in boninites; Kamenetsky et al., 2001; Falloon et al., 2008) (Fig. 13C). The FeO/MgO of the parental melts in equilibrium with high Cr# spinels varies between ~0.5 and 1.5 (Fig. 13C). The inferred parental melt composition in equilibrium with the low Cr# chromitites has high Al_2O_3 content (15.9–16.5 wt.%) and nearly constant FeO/MgO (1.1–1.3), which is very similar to MORB magmas (Al_2O_3 ~15 wt.%; Kamenetsky et al., 2001) (Fig. 13C).

6.4. Geodynamic implications: nascent arc magmatism?

The observed compositional variations provide evidence for understanding the magmatic evolution of Neotethyan arc system that could explain the coexistence of geochemically diverse MORB-like and SSZ-like melts in the Sabzevar ophiolite. More work is needed to understand the crustal sequence of this ophiolite including cumulate gabbros and overlying lavas to confirm this. Existing data (e.g., Maleki, 2013) confirm the presence of island-arc tholeiitic (IAT) and calc-alkaline magmatic rocks in the Sabzevar ophiolite crustal sequence. Temporal relationships in the Sabzevar mantle sequence show that plagioclase–Cpx impregnations (melt pocket-shaped domains) are early events, crosscut by dunites and high Cr-chromitites. Field observations show that low Cr# chromitites are older than high-Cr# chromitites. Late stage, arc-related and depleted wehrlitic dikes crosscut all units. The observed scenario is early tholeiites and late boninites, as revealed in chromitite compositions as well as mantle rocks and dikes. The origin of bimodal compositional variations of podiform chromitites is commonly ascribed to differences in the composition of the melts from which chromian spinels were precipitate. Differences in melt compositions may be related to (i) different degrees of partial melting (Arai, 1992); and (ii) melt–rock interaction with variably depleted peridotites (e.g., Zhou and Robinson, 1997; Zhou et al., 2005). The combination of these two factors affects supra-subduction zone ophiolites due to variable fluid fluxes coming from down-going slab. Water plays an important role in forming podiform chromitites in arc settings (Gaetani et al., 1994; Matveev and Ballhaus, 2002), hence chromian spinel is stabilized relative to silicate phases in more hydrous basaltic magmas (Gaetani et al., 1994); otherwise the Cr solubility in the mafic melts is sensitive to oxygen fugacity (Roeder and Reynolds, 1991). Favorable conditions are available in sub-arc setting, where high Cr# podiform chromitites occur (e.g., Arai, 1994; Arai and Yurimuto, 1995).

Boninitic melt may be responsible for forming high Cr# podiform chromitites. Chromian spinels with high Cr# (>0.6) are frequently found in boninitic magmatic rocks from arc settings, whereas rocks formed at mid-oceanic ridge setting contain spinels with 0.1–0.5 Cr# (Dick and Bullen, 1984; Arai, 1997a, 1997b, 2011). We believe that low Cr# chromitites formed through reaction of early arc, MORB-like magmas (perhaps FAB of Reagan et al., 2010) with harzburgitic wall rocks whereas high Cr# chromitites precipitated from arc-related boninitic melts, similar to the scenario described by Ahmed and Arai (2002) and Miura et al. (2012). Early tholeiitic melts impregnated the Baghjar-Kuh Siah mantle rocks with plagioclase–clinopyroxene (Fig. 15). The formation of these podiform chromitites is related to focused channeling of partial melts in a supra-subduction zone setting during growth of a nascent arc (Fig. 15).

Geological and geochemical studies on several Tethyan ophiolites as well as IBM forearc have revealed the presence of distinct peridotite units within these mantle sequences, including mid-oceanic ridge-like and a highly refractory suites (e.g., Morishita et al., 2011; Aldanmaz et al., 2012; Uysal et al., 2012). These geochemical observations are thought to reflect progressive evolution from a mid-oceanic ridge to a supra-subduction zone setting for Tethyan ophiolites (Aldanmaz et al., 2009, 2012; Uysal et al., 2012). In this scenario, plagioclase lherzolites are refertilized due to percolating MORB melts beneath a spreading center, whereas depleted harzburgites and dunites reflect more extensive mantle melting as a result of a more hydrous environment. We suggest that MORB-like melts interacted with Sabzevar ophiolite mantle sequences during subduction initiation and that these melts precipitated low Cr# chromitites and plagioclase–clinopyroxene impregnations (melt-pocket shaped domains) (Fig. 15). This is the mantle expression of the 'subduction initiation rule', articulated for well-studied ophiolite volcanic sections by Whattam and Stern (2011), whereby subduction initiation (SI) is manifested by outpourings of tholeiitic (FAB-like) basalts followed by calc-alkaline and/or boninitic melts. Upwelling of asthenospheric mantle in the forearc region during early SI first causes decompression melting of upwelling asthenospheric mantle to form MORB-like melts (FAB of Reagan et al., 2010; Ishizuka et al., 2011). Such magmas produced early diabasic dikes, impregnated plagioclase lherzolites, and low-Cr# podiform chromitites. Production of FAB during early SI is commonly followed by generation of arc-like or boninitic melts as slab-derived fluids eventually reach the zone of melt generation in the mantle wedge as the sinking slab descends further. These later boninitic melts produced Sabzevar replacive dunites, high Cr# chromitites and depleted, arc related intrusive dikes including wehrlites.

7. Conclusions

Sabzevar ophiolite ultramafic exposures including impregnated lherzolites, depleted peridotites, dunites and podiform chromitites are a well-preserved upper mantle sequence including Moho Transition Zone that also may be a snapshot of how the mantle responds when a new subduction zone forms. Lherzolites were affected by plagioclase–clinopyroxene impregnations and contain high Ti, Na and REE clinopyroxenes similar to those of abyssal peridotites. Mantle harzburgites far from impregnations contain depleted clinopyroxenes, similar to those of supra-subduction zone peridotites. High Cr# chromitites dominate in the Sabzevar ophiolite mantle section whereas low Cr# chromitites are less abundant. The formation of Sabzevar

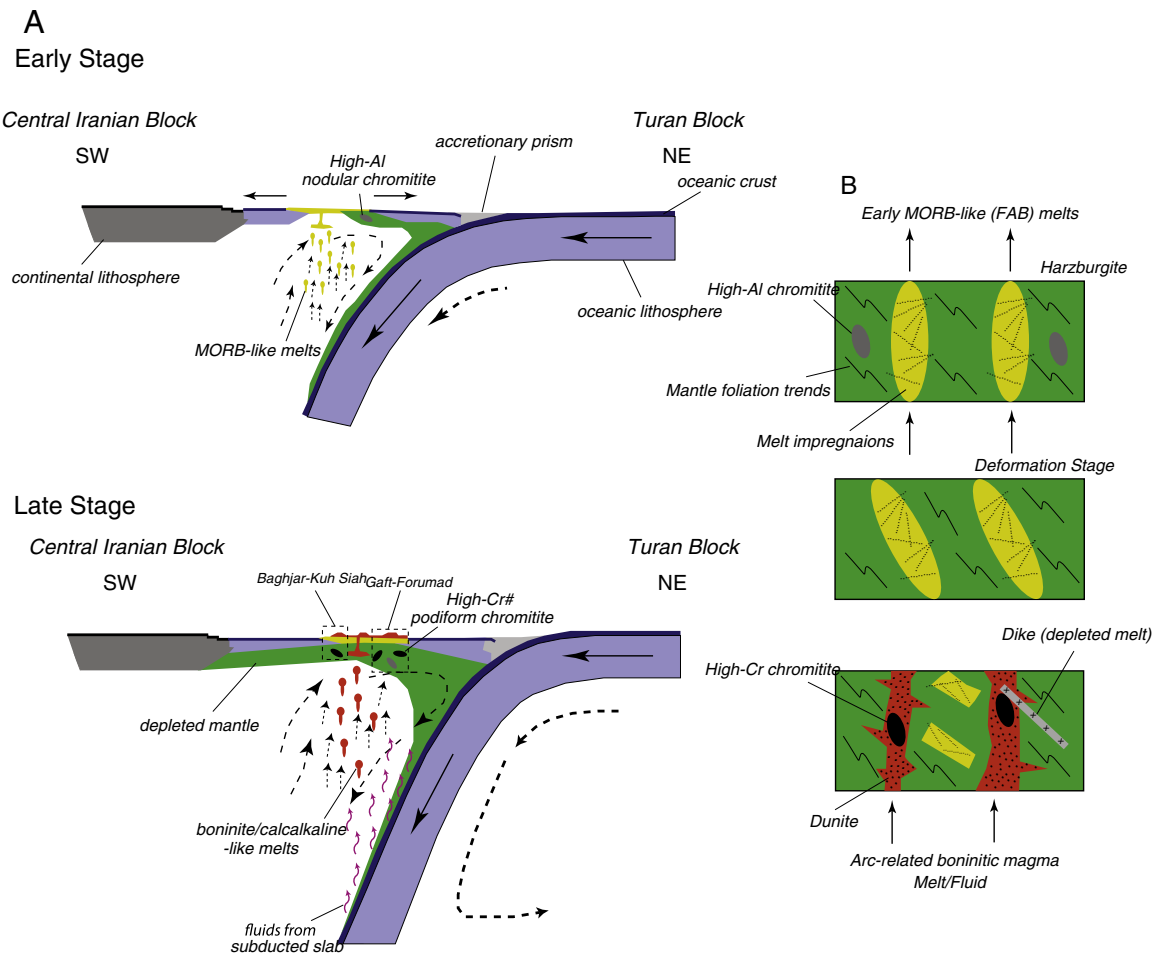

Fig. 15. A — Schematic model for tectono-magmatic evolution and genesis of impregnated peridotites, high Cr# and low Cr# chromitites and depleted residual mantle rocks in the Sabzevar mantle section. B — Schematic evolution of the Sabzevar ophiolite upper mantle. Plagioclase lherzolites were produced in an early stage of subduction while depleted harzburgites, dunites and high Cr# chromitites are formed in later stage with interaction with fluids coming off the subducted slab (modified after Arai et al., 2006).

ophiolite podiform chromitites is related to the melt/mantle interactions, with early tholeiitic melts responsible for precipitating low Cr# chromitites and late boninitic melts forming high Cr# chromitites.

Supplementary data to this article can be found online at http://dx.doi.org/10.1016/j.gr.2013.09.007.

Acknowledgments

This research was funded by Kanazawa University (Japan) to the first author (HSM). Partial support from Damghan University (Iran) is acknowledged. We thank Paul Robinson for inviting us to join this scientific discussion on the origin and significance of ophiolitic peridotite and chromitite. We are very grateful to Yildirim Dilek and Ercan Aldanmaz for their constructive reviews of the manuscript. Editorial suggestions by Prof. Santosh are highly appreciated.

References

Ahmed, A.H., Arai, S., 2002. Unexpectedly high-PGE chromitite from the deeper mantle section of the northern Oman ophiolite and its tectonic implications. Contributions to Mineralogy and Petrology 143, 263–278.

Ahmed, A.H., Harbi, H.M., Habtoor, A.M., 2012. Compositional variations and tectonic settings of podiform chromitites and associated ultramafic rocks of the Neoproterozoic ophiolite at Wadi Al Hwanet, northwestern Saudi Arabia. Journal of Asian Earth Sciences 56, 118–134.

Akizawa, N., Arai, S., Tamura, A., 2012. Behavior of MORB magmas at uppermost mantle beneath a fast-spreading axis: an example from Wadi Fizh of the northern Oman ophiolite. Contributions to Mineralogy and Petrology 164, 601–625.

Alavi, M., 1991. Sedimentary and structural characteristics of the Paleo-Tethys remnants in northeastern Iran. Geological Society of America Bulletin 103, 983–992.

Aldanmaz, E., Schmidt, M.W., Gourgaud, A., Meisel, T., 2009. Mid-ocean ridge and supra-subduction geochemical signatures in spinel-peridotites from the Neotethyan ophiolites in SW Turkey: implications for upper mantle melting processes. Lithos 113, 691–708.

Aldanmaz, E., Meisel, T., Celik, O.F., Henjes-Kunst, F., 2012. Osmium isotope systematics and highly siderophile element fractionation in spinel-peridotites from the Tethyan ophiolites in SW Turkey: implications for multi-stage evolution of oceanic upper mantle. Chemical Geology 294–295, 152–164.

Arai, S., 1980. Dunite–harzburgite–chromitite complexes as refractory residue in the Sangun Yamaguchi zone, western Japan. Journal of Petrology 21, 141–165.

Arai, S., 1992. Petrology of peridotites as a tool of insight into mantle processes: a review. Journal of Mineralogy and Petrology 87, 351–363 (in Japanese with English abstract).

Arai, S., 1994. Compositional variation of olivine–chromian spinel in Mg-rich magmas as a guide to their residual spinel peridotites. Journal of Volcanology and Geothermal Research 59, 279–294.

Arai, S., 1997a. Control of wall-rock composition on the formation of podiform chromitites as a result of magma/peridotite interaction. Resource Geology 47, 177–187.

Arai, S., 1997b. Origin of podiform chromitites. Journal of Asian Earth Sciences 15, 303–310.

Arai, S., Abe, N., 1994. Possible presence of podiform chromitite in the arc mantle: chromitite xenoliths from the Takashima alkali basalt, southwest Japan arc. Mineralium Deposita 29, 434–438.

Arai, S., Takemoto, Y., 2007. Mantle wehrlite from Hess Deep as a crystal cumulate from an ultra-depleted primary melt in East Pacific Rise. Geophysical Research Letters 34. http://dx.doi.org/10.1029/2006GL029198 L08302.

Arai, S., Yurimoto, H., 1994. Podiform chromitites of the Tari-Misaka ultramafic complex, southwestern Japan, as mantle–melt interaction products. Economic Geology 89, 1279–1288.

Arai, S., Yurimuto, H., 1995. Possible sub-arc origin of podiform chromitites. The Island Arc 4, 104–111.

Arai, S., Matsukage, K., Isobe, E., Vysotskiy, S., 1997. Concentration of incompatible elements in oceanic mantle: effect of melt/wall interaction in stagnant or failed melt conduits within peridotite. Geochimica et Cosmochimica Acta 61, 671–675.

Arai, S., Takda, S., Michibayashi, K., Kida, M., 2004. Petrology of peridotite xenoliths from Iraya Volcano, Philippines, and its implication for dynamic mantle–wedge processes. Journal of Petrology 45, 369–389.

Arai, S., Kadoshima, K., Morishita, T., 2006. Widespread arc-related melting in the mantle section of the northern Oman ophiolite as inferred from detrital chromian spinels. Journal of Geological Society, London 163, 869–879.

Arai, S., Hawke, B.R., Giguere, T.A., Misawa, K., Miyamoto, M., Kojima, H., 2010. Antarctic lunar meteorites Yamato-793169, Asuka-881757, MIL 05035, and MET 01210 (YAMM): launch pairing and possible cryptomare origin. Geochimica et Cosmochimica Acta 74, 2231–2248.

Arai, S., Okamura, H., Kadoshima, K., Tanaka, C., Suzuki, S., Ishimura, S., 2011. Chemical characteristics of chromian spinel in plutonic rocks: implications for deep magma processes and discrimination of tectonic setting. Island Arc 20, 125–137.

Baroz, F., Macaudiere, E.J., 1984. La serie volcanosedimentaire du chainon ophiolitique de Sabzevar (Iran). Ofioliti 9 (01), 3–26.

Benn, K., Nicolas, A., Reuber, I., 1988. Mantle–crust transition zone and origin of wehrlitic magmas: evidence from the Oman ophiolite. Tectonophysics 151, 75–85. http://dx.doi.org/10.1016/0040-1951(88)90241-7.

Berberian, M., King, G.C.P., 1981. Towards a paleogeography and tectonic evolution of Iran. Canadian Journal of Earth Sciences 18, 210–265.

Bizimis, M., Salters, V.J.M., Bonatti, E., 2000. Trace and REE content of clinopyroxenes from supra-subduction zone peridotites. Implications for melting and enrichment processes in island arcs. Chemical Geology 165, 67–85.

Bloomer, S.H., Hawkins, J.W., 1983. Gabbroic and ultramafic rocks from the Mariana Trench: an island arc ophiolite. In: Hayes, D.E. (Ed.), The Tectonic and Geologic Evolution of Southeast Asian Seas and Islands Part 2. Geophysical Monograph, vol. 27. American Geophysical Union, Washington, DC, USA, pp. 94–317.

Cassard, D., Nicolas, A., Rabinowith, M., Moutte, J., Leblanc, M., Prinzhofer, A., 1981. Structural classification of chromite pods in southern New Caledonia. Economic Geology 76, 805–831.

Dick, H.J.B., 1989. Abyssal peridotites, very slow spreading ridges and ocean ridge magmatism. In: Saunders, A.D., Norry, M.J. (Eds.), Magmatism in the Ocean Basins. Geological Society London, Special Publication, no. 42, pp. 71–105.

Dick, H.J.B., Bullen, T., 1984. Chromian spinel as a petrogenetic indicator in abyssal and Alpine-type peridotites and spatially associated lavas. Contributions to Mineralogy and Petrology 86, 54–76.

Dijkstra, A.H., Drury, M.R., Vissers, R.L.M., 2001. Structural petrology of plagioclase peridotites in the West Othris Mountains (Greece): melt impregnation in mantle lithosphere. Journal of Petrology 42, 5–24.

Elthon, D., 1992. Chemical trends in abyssal peridotites: refertilization of depleted suboceanic mantle. Journal of Geophysical Research 97, 9015–9025.

Falloon, T.J., Green, D.H., Danyushevsky, L.V., McNeill, A.W., 2008. The composition of near-solidus partial melts of fertile peridotites at 1 and 1.5 GPa: implications for the petrogenesis of MORB. Journal of Petrology 49, 591–613.

Gaetani, G.A., Grove, T.L., Bryan, W.B., 1994. Experimental phase relations of basaltic andesite from Hole 839B under hydrous conditions. In: Hwkinds, J., Parson, L., Allan, J. (Eds.), Proceedings of the Ocean Drilling Program. Scientific Results, 135, pp. 557–653.

Ghiorso, M.S., Hirschmann, M.M., Reiners, P.W., Kress III, V.C., 2002. The pMELTS: a revision of MELTS aimed at improving calculation of phase relations and major element partitioning involved in partial melting of the mantle at pressures up to 3 GPa. Geochemistry, Geophysics, Geosystems 3 (5). http://dx.doi.org/10.1029/2001GC000217.

Hart, S.R., Dunn, T., 1993. Experimental Cpx/melt partitioning of 24 trace elements. Contributions to Mineralogy and Petrology 113, 1–8.

Hellebrand, E., Snow, J.E., Dick, H.J.B., Hofmann, A.W., 2001. Coupled major and trace elements as indicators of the extent of melting in mid-ocean ridge peridotites. Nature 410, 677–681.

Hellebrand, E., Snow, J.E., Muhe, R., 2002. Mantle melting beneath Gakkel Ridge (Arctic Ocean): abyssal peridotite spinel compositions. Chemical Geology 182, 227–235.

Hellebrand, E., Snow, J.E., Mostefaoui, S., Hoppe, P., 2005. Trace element distribution between orthopyroxene and clinopyroxene in peridotites from the Gakkel Ridge: a SIMS and NanoSIMS study. Contributions to Mineralogy and Petrology 150, 486–504.

Hock, M., Friedrich, G., Pluger, W.L., Wichowski, A., 1986. Refractory and metallurgical type chromite ores, Zambales ophiolite, Luzon, Philippines. Mineralium Deposita 21, 190–199.

Ishii, T., Robinson, P.T., Maekawa, H., Fiske, R., 1992. Petrological studies of peridotites from diapiric serpentinite seamounts in the Izu-Ogasawara-Mariana forearc, Leg 125. In: Fryer, P., Pearce, J.A., Stokking, L.B., et al. (Eds.), Proc. ODP. Sci. Results, 125. Ocean Drilling Program, College Station, TX, pp. 445–485.

Ishizuka, O., Tani, K., Reagan, M.K., Kanayama, K., Umino, S., Sakamoto, I., Harigane, Y., Miyajima, Y., Yuasa, M.J., Dunkley, D.J., 2011. The timescales of subduction initiation and subsequent evolution of an oceanic island arc. Earth and Planetary Science Letters 306, 229–240.

Johnson, K.T.M., Dick, H.J.B., 1992. Open system melting and temporal and spatial variation of peridotite and basalt at the Atlantic II fracture zone. Journal of Geophysical Research 97, 9219–9241.

Johnson, K.T.M., Dick, H.J.B., Shimizu, N., 1990. Melting in the oceanic upper mantle: an ion microprobe study of diopsides in abyssal peridotites. Journal of Geophysical Research 95, 2661–2678.

Kamenetsky, V.S., Crawford, A.J., Meffre, S., 2001. Factors controlling chemistry of magmatic spinel: an empirical study of associated olivine, Cr-spinel and melt inclusions from primitive rocks. Journal of Petrology 42, 655–671.

Kelemen, P.B., Dick, H.J.B., Quick, J.E., 1992. Formation of harzburgite by pervasive melt–rock reaction in the upper mantle. Nature 358, 635–641.

Kelemen, P.B., Shimizu, N., Salters, V.J.M., 1995. Extraction of mid-ocean-ridge basalt from the upwelling mantle by focused flow of melt in dunite channels. Nature 375, 747–753.

Kelemen, P.B., Hirth, G., Shimizu, N., Spiegelman, M., Dick, H.J.B., 1997. A review of melt migration processes in the adiabatically upwelling mantle beneath spreading ridges. Philosophical Transactions of the Royal Society of London A 355, 283–318.

Koepke, J., Schoenborn, S., Oelze, M., Wittmann, H., 2009. Petrogenesis of crustal wehrlites in the Oman ophiolite: experiments and natural rocks. Geochemistry, Geophysics, Geosystems (G3) 10, 1–26. http://dx.doi.org/10.1029/2009GC002488 (Q10002).

Koga, K.T., Kelemen, P.B., Shimizu, N., 2001. Petrogenesis of the crust–mantle transition zone and the origin of lower crustal wehrlite in the Oman ophiolite. Geochemistry, Geophysics, Geosystems (G3), 2(9). http://dx.doi.org/10.1029/2000GC000132 (1038).

Leblanc, M., Ceuleneer, G., 1992. Chromite crystallization in a multicellular magma flow evidence from a chromitite dike in the Oman ophiolite. Lithos 27, 231–257.

Leblanc, M., Violette, J.F., 1983. Distribution of Al-rich and Cr-rich chromite pods in ophiolites. Economic Geology 78, 293–301.

Lensch, G., 1980. Major element geochemistry of the ophiolites in north-eastern Iran. In: Panayiotou, A. (Ed.), Proceedings to International Ophiolite Symposium. Geological Survey Department, Republic of Cyprus, pp. 398–401.

Loucks, R.R., 1996. A precise olivine–augite Mg–Fe-exchange geothermometer. Contributions to Mineralogy and Petrology 125, 140–150.

Maleki, L., 2013. Geochemistry and Petrogenesis of Plagiogranites and Host Rocks in the Sabzevar Ophiolite. (M.Sc. Thesis) Damghan University (in Farsi with English abstract).

Matveev, S., Ballhaus, C., 2002. Role of water in the origin of podiform chromitite deposits. Earth and Planetary Science Letter 203, 235–243.

Maurel, C., Maurel, P., 1982. Etude experimentale de equilibre Fe2 + –Fe3+ dans les spinelles chromifieres et les liquides silicates basiques coexistants, a 1 atm. C. R. Academic Sciences (Paris) 295, 209–212.

Merlini, A., Grieco, M., Ottolini, L., Diella, V., 2011. Probe and SIMS investigation of clinopyroxene inclusions in chromites from the Troodos chromitites (Cyprus): implications for dunite–chromitite genesis. Ore Geology Reviews 41, 22–34.

Miura, M., Arai, S., Ahmed, A.H., Mizukami, T., Okuno, M., Yamamoto, S., 2012. Podiform chromitite classification revisited: a comparison of discordant and concordant chromitite pods from Wadi Hilti, northern Oman ophiolite. Journal of Asian Earth Sciences 59, 52–61.

Morishita, T., Ishida, Y., Arai, S., 2005. Simultaneous determination of multiple trace element compositions in thin (b30 μm) layers of BCR-2G by 193 nm ArF excimer laser ablation-ICP-MS: implications for matrix effect and element fractionation on quantitative analysis. Geochemical Journal 39, 327–340.

Morishita, T., Dilek, Y., Shallo, M., Tamura, A., Arai, S., 2011. Insight into the uppermost mantle section of a maturing arc: the Eastern Mirdita ophiolite, Albania. Lithos 124, 215–226.

Nicolas, A., 1989. Structure of Ophiolites and Dynamics of Oceanic Lithosphere. Kluwer Academic Publication (367 pp.).

Niu, Y., Langmuir, C.H., Kinzler, R.J., 1997. The origin of abyssal peridotites: a new perspective. Earth and Planetary Science Letter 152, 251–265.

Noghreyan, M.K., 1982. Evolution geochimique, mineralogique et structurale d'un edifice ophiolitique singulier: le massif de Sabzevar (partie centrale). (NE de l'Iran. These Doc. d'Etat) Universite de Nancy, France.

Obata, M., Banno, S., Mori, T., 1974. The iron–magnesium partitioning between naturally occurring coexisting olivine and Ca-rich clinopyroxene: an application of the simple mixture model to olivine solid solution. Bulletin de Societe du France, Mineralogy Cristallography 97, 101–107.

Ottley, C.J., Pearson, D.G., Irvine, G.J., 2003. A routine method for the dissolution of geological samples for the analysis of REE and trace elements via ICP-MS. In: Holland, J.G., Taner, S.D. (Eds.), Plasma Source Mass Spectrometry. Applications and Emerging Technologies, The Royal Society of Chemistry, pp. 221–230.

Paktunc, D., 1990. Origin of podiform chromite deposits by multistage melting, melt segregation and magma mixing in the upper mantle. Ore Geology Reviews 5, 211–222.

Parkinson, I.J., Pearce, J.A., 1998. Peridotites from the Izu–Bonin–Mariana forearc (ODP Leg 125): evidence for mantle melting and melt–mantle interaction in a supra-subduction zone setting. Journal of Petrology 39, 1577–1618.

Pearce, J.A., Barker, P.F., Edwards, S.J., Parkinson, I.J., Leat, P.T., 2000. Geochemistry and tectonic significance of peridotites from the South Sandwich arc-basin systems, South Atlantic. Contributions to Mineralogy and Petrology 139, 36–53.

Pearce, J.A., Parkinson, I.J., 1993. Trace element models for mantle melting: application to volcanic arc petrogenesis. Geological Society, London, Special Publications 76, 373–403.

Piccardo, G.B., Zanetti, A., Müntener, O., 2007. Melt/peridotite interaction in the Lanzo South peridotite: field, textural and geochemical evidence. Lithos 94 (1–4), 181–209. http://dx.doi.org/10.1016/j.lithos.2006.07.002.

Potts, P.J., Tindle, A.G., Webb, P.C., 1992. Geochemical Reference Materials Compositions, Rocks, Minerals, Sediments, Soils, Carbonates, Refractories and Ores Used in Research and Industry. Whittles Publishing, Caithness.

Reagan, M.K., Ishizuka, O., Stern, R.J., Kelley, K.A., Ohara, Y., Blichert-Toft, J., Bloomer, S.H., Cash, J., Fryer, P., Hanan, B.B., Hickey-Vargas, R., Ishii, T., Kimura, J.I., Peate, D.W., Rowe, M.C., Woods, M., 2010. Fore-arc basalts and subduction initiation in the Izu–Bonin–Mariana system. Geochemistry, Geophysics, Geosystems (G3) 11. http://dx.doi.org/10.1029/2009GC002871 (Q03X12).

Robinson, A., Yin, A., Manning, C., Harrison, T.M., Zhang, S., Wang, X., 2004. Tectonic evolution of the northeastern Pamir: constraints from the northern portion of the Cenozoic Kongur Shan extensional system, western China. Geological Society of America Bulletin 116, 953–973.

Roeder, P.L., Reynolds, I., 1991. Crystallization of chromite and chromium solubility in basaltic melts. Journal of Petrology 32, 909–934.

Rollinson, H., Adetunji, J., 2013a. Mantle podiform chromitites do not form beneath mid-ocean ridges: a case study from the Moho transition zone of the Oman ophiolite. Lithos 177, 314–327.
Rollinson, H., Adetunji, J., 2013b. The geochemistry and oxidation state of podiform chromitites from the mantle section of the Oman ophiolite: a review. Gondwana Research 27, 543–554.
Ross, K., Elthon, D., 1993. Cumulates from strongly depleted mid-ocean basalt. Nature 365, 826–829.
Rossetti, F., Theye, T., Lucci, F., Bouybaouene, M.L., Dini, A., Gerdes, A., Phillips, D., Cozzupoli, D., 2010. Timing and modes of granite magmatism in the core of the Alboran domain, Rif chain, northern Morocco: implications for the Alpine evolution of the western Mediterranean. Tectonics 29. http://dx.doi.org/10.1029/2009TC002487 TC2017.
Sano, S., Kimura, J., 2007. Clinopyroxene REE geochemistry of the Red Hills peridotite, New Zealand: interpretation of magmatic processes in the upper mantle and in the Moho Transition Zone. Journal of Petrology 48 (1), 113–139. http://dx.doi.org/10.1093/petrology/egl056.
Sengor, A.M.C., 1990. A new model for the late Paleozoic–Mesozoic tectonic evolution of Iran and implications for Oman. In: Robertson, A.H.F., Searle, M.P., Ries, A.C. (Eds.), The Geology and Tectonics of the Oman Region. Geological Society, London, Special Publications, 49, pp. 797–831.
Seyler, M., Bonatti, E., 1997. Regional-scale melt–rock interaction in lherzolitic mantle in the Romanche fracture zone Z Atlantic Ocean. Earth and Planetary Science Letters 146, 273–287.
Shafaii Moghadam, H., 2009. The Nain-Baft Ophiolites (Central Iran): Age, Structure and Origin. (Ph.D. thesis) Shahid Beheshti University, Tehran, Iran (532 pp.).
Shi, R., Griffin, W.L., O Reilly, S.Y., Huange, Q., Zhang, X., Liu, D., Zhi, X., Xia, Q., Ding, L., 2012. Melt/mantle mixing produces podiform chromite deposits in ophiolites: implications of Re–Os systematics in the Dongqiao Neo-Tethyan ophiolite, northern Tibet. Gondwana Research 21, 194–206.
Shojaat, B., Hassanipak, A.A., Mobasher, K., Ghazi, A.M., 2003. Petrology, geochemistry and tectonics of the Sabzevar ophiolite, north central Iran. Journal of Asian Earth Sciences 21, 1053–1067.
Sobolev, A.V., Shimizu, N., 1993. Ultra-depleted primary melt included in an olivine from the Mid-Atlantic Ridge. Nature 363, 151–154.
Stern, R.J., 2004. Subduction initiation: spontaneous and induced. Earth and Planetary Science Letters 226, 275–292.
Stern, R.J., 2010. The anatomy and ontogeny of modern intra-oceanic arc systems. In: Kusky, T.M., Zhai, M.G., Xiao, W. (Eds.), The Evolving Continents: Understanding Processes of Continental Growth. Geological Society of London, Special Publication, no. 338, pp. 7–34.
Stern, R.J., Bloomer, S.H., 1992. Subduction zone infancy; examples from the Eocene Izu–Bonin–Mariana and Jurassic California arcs. Geological Society of America Bulletin 104, 1621–1636.
Sun, S.S., Mcdonough, W.F., 1989. Chemical and isotopic systematics of oceanic basalts: implications for mantle composition and processes. In: Saunders, A.D., Norry, M.J. (Eds.), Magmatism in the Ocean Basins. Geological Society, London, Special Publications, 42, pp. 313–345.
Takahashi, E., 1980. Thermal history of iherzolite xenoliths-I. Petrology of iherzolite xenoliths from the Ichinomegata Crater, Oga peninsula, northeast Japan. Geochimica et Cosmochimica Acta 44, 1643–1658.
Takahashi, E., Uto, K., Schilling, J.G., 1987. Primary magma compositions and Mg/Fe ratios of their mantle residues along Mid-Atlantic Ridge 29N to 73N. Tec Rep Inst Stud Earth's Inter Okayama Univ Ser A, 9, pp. 1–14.
Tamura, A., Arai, S., 2006. Harzburgite–dunite–orthopyroxenite suite as a record of supra-subduction zone setting for the Oman ophiolite mantle. Lithos 90, 43–56.
Tamura, A., Arai, S., Ishimaru, S., Andal, E.S., 2008. Petrology and geochemistry of peridotites from IODP Site U1309 at Atlantis Massif, MAR 30°N: micro- and macroscale melt penetrations into peridotites. Contributions to Mineralogy and Petrology 155, 491–509.
Uesugi, J., Arai, S., Morishita, T., Matsukage, K., Kadoshima, K., Tamura, A., Abe, N., 2003. Significance and variety of mantle-crust boundary in the Oman ophiolite. Journal of Geography 112, 750–768 (in Japanese with English abstract).
Uysal, E., Ersoy, E.Y., Karsli, O., Dilek, Y., Sadiklar, M.B., Ottely, C.J., Tiepolo, M., Meisel, T., 2012. Coexistence of abyssal and ultra-depleted SSZ type mantle peridotites in a Neo-Tethyan Ophiolite in SW Turkey: Constraints from mineral composition, whole-rock geochemistry (major–trace–REE–PGE), and Re–Os isotope systematics. Lithos 132–133, 50–69.
Whattam, S.A., Stern, R.J., 2011. The 'subduction initiation rule': a key for linking ophiolites, intra-oceanic forearcs and subduction initiation. Contributions to Mineralogy and Petrology 162, 1031–1045.
Yamamoto, J., Nishimura, K., Sugimoto, T., Takemura, K., Takahata, N., Sano, Y., 2009. Diffusive fractionation of noble gases in mantle with magma channels: origin of low He/Ar in mantle-derived rocks. Earth and Planetary Science Letters 280, 167–174.
Yang, J.S., Zhang, R.Y., Li, T.F., Zhang, Zh.M., Liou, J.G., 2007. Petrogenesis of the garnet peridotite and garnet-free peridotite of the Zhimafang ultramafic body in the Sulu ultrahigh-pressure metamorphic belt, eastern China. Journal of Metamorphic Geology 25, 187–206.
Zaki Khedr, M., Arai, S., Python, M., Tamura, A., 2013. Chemical variations of abyssal peridotites in the central Oman ophiolite: evidence of oceanic mantle heterogeneity. Gondwana Research 25, 1242–1262.
Zhou, M.F., Robinson, P.T., 1994. High-Cr and high-Al chromitites, western China: relationship to partial melting and melt/rock interaction in the upper mantle. International Geology Review 36, 678–686.
Zhou, M.F., Robinson, P.T., 1997. Origin and tectonic setting of podiform chromite deposits. Economic Geology 92, 259–262.
Zhou, M.F., Robinson, P.T., Malpas, J., Li, Z., 1996. Podiform chromitites from the Luobusa ophiolite (southern Tibet): implications for melt/rock interaction and chromite segregation in the upper mantle. Journal of Petrology 37, 3–21.
Zhou, M.F., Sun, M., Keays, R., Kerrich, R., 1998. Control on platinum group elemental distributions of podiform chromitites: a case study of high Cr and high Al chromitites from Chinese orogenic belts. Geochimica et Cosmochimica Acta 62, 677–688.
Zhou, M.F., Robinson, P.T., Malpas, J., Aitchison, J., Sun, M., Bai, W.-J., Hu, X.F., Yang, J.S., 2001. Melt/mantle interaction and melt evolution in the Sartohay high-Al chromite deposit of the Dalabute ophiolite (NW China). Journal of Asian Earth Sciences 19, 517–534.
Zhou, M.F., Robinson, P.T., Malpas, J., Edwards, S.J., Qi, L., 2005. REE and PGE geochemical constraints on the formation of dunites in the Luobusa ophiolite, Southern Tibet. Journal of Petrology 46 (3), 615–639.